Journal of
Plankton Research

academic.oup.com/plankt

J. Plankton Res. (2021) 1–19. https://doi.org/10.1093/plankt/fbab049

BLOOFINZ - Gulf of Mexico

Constraining the sources of nitrogen fueling export production in the Gulf of Mexico using nitrogen isotope budgets

ANGELA N. KNAPP[1,*], RACHEL K. THOMAS[1], MICHAEL R. STUKEL[1], THOMAS B. KELLY[1], MICHAEL R. LANDRY[2], KAREN E. SELPH[3], ESTRELLA MALCA[4,5], TRIKA GERARD[5] AND JOHN LAMKIN[5]

[1]EOAS DEPARTMENT, FLORIDA STATE UNIVERSITY, 1011 ACADEMIC WAY, TALLAHASSEE, FL 32306, USA, [2]SCRIPPS INST. OF OCEANOGRAPHY, UNIVERSITY OF CALIFORNIA AT SAN DIEGO, 9500 GILMAN DR, LA JOLLA, CA 92093-0227, USA, [3]SCHOOL OF OCEAN AND EARTH SCIENCE AND TECHNOLOGY, DEPARTMENT OF OCEANOGRAPHY, UNIVERSITY OF HAWAI'I AT MANOA, 75 VIRGINIA BEACH DR, 1000 POPE ROAD, HONOLULU, HI 96822, USA, [4]COOPERATIVE INSTITUTE OF MARINE AND ATMOSPHERIC STUDIES, UNIVERSITY OF MIAMI, 4600 RICKENBACKER CSWY, MIAMI, FL 33149, USA AND [5]SOUTHEAST FISHERIES SCIENCE CENTER, NOAA NATIONAL MARINE FISHERIES SERVICE, 75 VIRGINIA BEACH DR, MIAMI, FL 33149 USA

*CORRESPONDING AUTHOR. anknapp@fsu.edu

Received October 13, 2020; editorial decision July 15, 2021; accepted July 15, 2021

Corresponding editor: Pia Moisander

The availability of nitrogen (N) in ocean surface waters affects rates of photosynthesis and marine ecosystem structure. In spite of low dissolved inorganic N concentrations, export production in oligotrophic waters is comparable to more nutrient replete regions. Prior observations raise the possibility that di-nitrogen (N_2) fixation supplies a significant fraction of N supporting export production in the Gulf of Mexico. In this study, geochemical tools were used to quantify the relative and absolute importance of both subsurface nitrate and N_2 fixation as sources of new N fueling export production in the oligotrophic Gulf of Mexico in May 2017 and May 2018. Comparing the isotopic composition ("δ^{15}N") of nitrate with the δ^{15}N of sinking particulate N collected during five sediment trap deployments each lasting two to four days indicates that N_2 fixation is typically not detected and that the majority ($\geq$80%) of export production is supported by subsurface nitrate. Moreover, no gradients in upper ocean dissolved organic N and suspended particulate N concentration and/or δ^{15}N were found that would indicate significant N_2 fixation fluxes accumulated in these pools, consistent with low *Trichodesmium* spp. abundance. Finally, comparing the δ^{15}N of sinking particulate N captured within vs. below the euphotic zone indicates that during late spring regenerated N is low in δ^{15}N compared to sinking N.

KEYWORDS: Gulf of Mexico; δ15N budget; nitrate δ15N; regenerated production

available online at academic.oup.com/plankt

INTRODUCTION

Primary productivity in the ocean accounts for roughly half of annual global carbon (C) fixation. Despite low concentrations of inorganic forms of nitrogen (N), such as nitrate (NO_3^-) and ammonium (NH_4^+), in many parts of the low-latitude surface ocean, significant rates of C fixation occur in these seemingly nutrient impoverished regions (Emerson, 2014). Phytoplankton carrying out this photosynthesis not only play a crucial role in the global C cycle, and thus impact climate, but create the foundation of the marine food web. Two sources of N that fuel "new" primary production are NO_3^-, the dominant bioavailable form of N in the global ocean, and biologically mediated di-nitrogen (N_2) fixation (Dugdale & Goering, 1967). New production fueled by subsurface NO_3^- in mid- to high-latitude waters is supported by vertical mixing as thermocline stability erodes seasonally, with N_2 fixation thought to be more important in thermally stratified low-latitude surface waters. This "new" production is contrasted with photosynthesis supported by NH_4^+, known as "regenerated" production, that largely cycles in the surface ocean and does not contribute to export (Dugdale & Goering, 1967, Eppley & Peterson, 1979). While the distribution and rates of N_2 fixation in the ocean play a central role in regulating the fertility and community structure of marine ecosystems, these first-order properties of marine N_2 fixation remain poorly constrained. The highest short-term rates of N_2 fixation have been documented in the tropical North Atlantic (Mahaffey *et al.*, 2005, Sohm *et al.*, 2011) as well as the western tropical South Pacific (Caffin *et al.*, 2018, Knapp *et al.*, 2018b). The spatial distribution of elevated $^{15}N_2$ incubation-based N_2 fixation rates (Luo *et al.*, 2012) are consistent with both the preference of diazotrophs for warm waters (Breitbarth *et al.*, 2007, Stal, 2009) as well as the high atmospheric dust flux to the North Atlantic (Mahowald *et al.*, 2009, Prospero, 1996) that helps fulfill the significant iron requirement of the enzyme, nitrogenase, that catalyzes N_2 fixation (Berman-Frank *et al.*, 2001, Kustka *et al.*, 2003). However, field observations are spatially limited, leaving modeling efforts to identify the regions of the global ocean supporting the largest N_2 fixation fluxes underconstrained.

Both N_2 fixation rates and fluxes of subsurface NO_3^- to surface waters are expected to respond to global change (Capotondi *et al.*, 2012, Luo *et al.*, 2019, Shi *et al.*, 2012), underscoring the importance of accurately characterizing their roles in supporting low-latitude C fixation. Although incubation-based estimates of NO_3^- uptake and N_2 fixation rates are commonly used to evaluate their respective roles in surface waters (Shiozaki *et al.*, 2018), these measurements have limitations, including potential bottle effects (Westberry *et al.*, 2012), the inherent short-term nature of the measurements, and challenges in consistently implementing methodological protocols (White *et al.*, 2020). While incubation-based approaches are valuable, geochemical methods to evaluate NO_3^- vs. N_2 fixation fueled export complement our understanding of this process. One geochemical tool to quantify relative and absolute contributions of subsurface NO_3^- and N_2 fixation to export production relies on the distinct isotopic compositions ("$\delta^{15}N$") of these two N sources ("$\delta^{15}N$", where $\delta^{15}N = \{[(^{15}N/^{14}N)_{sample}/(^{15}N/^{14}N)_{reference}]—1\}\times 1\,000$, with atmospheric N_2 as the reference). N_2 fixation introduces new N to the ocean with a $\delta^{15}N$ of ~ -2 to 0‰ (Carpenter *et al.*, 1997, Hoering & Ford, 1960, Minagawa & Wada, 1986). In contrast, the $\delta^{15}N$ of NO_3^- mixed up from the subsurface in the western North Atlantic can range from 2 to 4‰ (Knapp *et al.*, 2008, Knapp *et al.*, 2005, Marconi *et al.*, 2015). Assuming these are the dominant inputs of new N to the euphotic zone, in steady state, the $\delta^{15}N$ of N fluxes out of the euphotic zone should reflect the relative importance of these N inputs. This "$\delta^{15}N$ budget" approach assumes that sinking particulate N (PN_{sink}) is the major flux of N out of the euphotic zone, and compares the $\delta^{15}N$ of subsurface NO_3^- and N_2 fixation with that of PN_{sink}.

Given these assumptions, the relative importance of each source of new N for supporting export production can be estimated using the two end-member mixing model described in Eqn. 1, where the fractional importance of N_2 fixation for supporting export production (x) is defined as:

$$PN_{sink}\delta^{15}N = x\left(-1‰\right) + (1-x)\left(NO_3^- + NO_2^-\delta^{15}N\right) \quad (1)$$

Rearranging and solving for x yields:

$$x = \left(NO_3^- + NO_2^-\delta^{15}N - PN_{sink}\delta^{15}N\right) / \left(1 + NO_3^- + NO_2^-\delta^{15}N\right) \quad (2)$$

Multiplying "x" by the PN_{sink} mass flux provides a time-integrated N_2 fixation rate that can be compared with $^{15}N_2$ incubation-based N_2 fixation rate measurements (Knapp *et al.*, 2016a).

Prior $\delta^{15}N$ budgets have been applied in oligotrophic waters like the Gulf of Mexico (GoM) where euphotic zone NO_3^- concentrations are low and N_2 fixation is thought to potentially support a significant (i.e. >10%) fraction of export production. Although N_2 fixation has recently been found to support the majority of export

production at one location in the southwest Pacific Ocean (Knapp *et al.*, 2018b), and in the eastern North Atlantic N_2 fixation has been found to support up to 40% of export (Bourbonnais *et al.*, 2009), even in regions where N_2 fixation rates are relatively high, $\delta^{15}N$ budgets indicate that subsurface NO_3^- fuels the majority of export production in the oligotrophic Atlantic and Pacific gyres (e.g. (Altabet, 1988, Casciotti *et al.*, 2008, Knapp *et al.*, 2016a, Knapp *et al.*, 2005)). Indeed, when $\delta^{15}N$ budgets do indicate N_2 fixation is a significant N source (Knapp *et al.*, 2018b), $^{15}N_2$ uptake rates (Caffin *et al.*, 2018) and diazotroph abundance (Stenegren *et al.*, 2018) are notably elevated and consistent with diazotroph "bloom" conditions that fall outside typical $^{15}N_2$ uptake observations (Luo *et al.*, 2012), thus leaving a clear signature when N_2 fixation is a quantitatively important source of new N supporting export production.

Typical $\delta^{15}N$ budget results appear consistent with related work indicating that not only is NO_3^- the dominant new N input to low-latitude surface waters, but that its distinct isotopic composition propagates through geochemical N pools as well as the food web of oligotrophic gyres. At the base of the food web, this has been shown near Bermuda where, even during stratified summer conditions, eukaryotes consuming NO_3^- are responsible for new production (Fawcett *et al.*, 2011). The importance of NO_3^- as a N source to the low-latitude ocean is also evident in the isotopic composition of dissolved organic nitrogen (DON). Phytoplankton release a fraction of new production as DON (Bronk & Ward, 1999, Bronk & Ward, 2000, Bronk & Ward, 2005, Ward & Bronk, 2001). The distinct $\delta^{15}N$ of surface ocean DON in the subtropical North Pacific versus the subtropical North Atlantic reflects the difference in $\delta^{15}N$ of subsurface NO_3^- of the two basins (Knapp *et al.*, 2011), again emphasizing the primary role of NO_3^- in supporting low-latitude production. Similarly, the $\delta^{15}N$ of suspended particulate N (PN_{susp}) in the surface ocean, a fraction of which includes living phytoplankton, also exhibits variations that track regional differences in the $\delta^{15}N$ of subsurface NO_3^-. For example, surface ocean PN_{susp} $\delta^{15}N$ ranges from 5 to 15‰ in regions with relatively high subsurface NO_3^- $\delta^{15}N$ such as in oxygen deficient zones (Knapp *et al.*, 2016a, White *et al.*, 2013). In contrast, the relatively low $\delta^{15}N$ of PN_{susp} in surface waters of the Sargasso Sea typically ranges from −1 to 0‰ (Altabet, 1988) and subsurface NO_3^- $\delta^{15}N$ is particularly low, 2 to 4‰ (Knapp *et al.*, 2008, Marconi *et al.*, 2017). Regional variations in subsurface NO_3^- $\delta^{15}N$ are also evident further up the food web in the $\delta^{15}N$ of zooplankton biomass, which is higher in the North Pacific (Hannides *et al.*, 2009) than North Atlantic (McClelland *et al.*, 2003).

While results from prior $\delta^{15}N$ budgets might lead to the expectation that subsurface NO_3^- is the dominant source of new N to GoM surface waters, the same environmental conditions that are thought to support significant rates of N_2 fixation in the tropical North Atlantic are also commonly found in the GoM. Modest N_2 fixation rates, up to 2.3 nmol N L^{-1} d^{-1}, have been measured on the West Florida Shelf (Mulholland *et al.*, 2006, Mulholland *et al.*, 2014) and off of the northern GoM shelf, 85 μmol N m^{-2} d^{-1} (Holl *et al.*, 2007), but the contribution of N_2 fixation to export production in the open waters of the GoM has not been quantified. Here we apply $\delta^{15}N$ budgets to evaluate the relative importance of subsurface NO_3^- and N_2 fixation for supporting export production in the oligotrophic GoM, as well as to estimate geochemically derived rates of N_2 fixation. A novel addition to these $\delta^{15}N$ budgets is the inclusion of estimates of zooplankton NH_4^+ and/or urea excretion as a secondary mechanism of N export from the euphotic zone.

METHODS

Sample collection

Samples were collected for inorganic nutrient concentration and isotopic analysis on the NOAA Ship *Nancy Foster* from 11 May to 29 May 2017 ("NF1704") and 30 April to 19 May 2018 ("NF1802") in the deep waters of the northern and central GoM (Fig. 1). Samples were also collected for DON concentration and isotopic analysis on the NF1802 cruise. Details of the cruises can be found in (Gerard *et al.*, In Review). Briefly, samples were collected during five Lagrangian experiments of 2–4-day duration (i.e. "cycles"), each initiated with the deployment of free-drifting, mixed-layer-drogued sediment traps and concluded with their recovery. The length of trap deployment was chosen to accommodate multiple cycles per cruise, with longer cycles conducted where patches of bluefin tuna larvae were observed. Cycles over the course of the two cruises were sequentially numbered, with the first three cycles on the 2017 cruise referenced as NF1704-C1 (C1), NF1704-C2 (C2) and NF1704-C3 (C3), and the two cycles on the 2018 cruise referenced as NF1802-C4 (C4) and NF1802-C5 (C5). During the Lagrangian experiments, water-column samples were collected from Niskin bottles deployed on a CTD-rosette close to the drifting sediment trap array at ~0200 local time each day. Nutrient samples were collected in the dark to accommodate predawn sampling for light incubation experiments (Yingling *et al.*, 2021). Nutrient samples passed an acid-cleaned 0.2-μm membrane filter and were stored

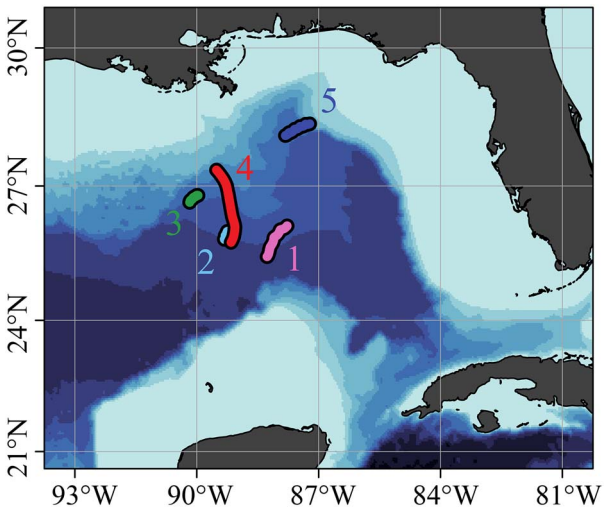

Fig. 1. Map of sampling locations for the 2017 (C1, pink, C2, light blue and C3, green) and 2018 (C4, red and C5, dark blue) cruises.

frozen at −20°C in acid-washed HDPE bottles for analysis on land, per GEOTRACES protocols (Cutter *et al.*, 2014). The depth of the mixed layer, defined as the depth at which density increased by 0.125 kg m^{-3} (Monterey & Levitus, 1997), ranged from 21 to 36 m during NF1704 (C1-C3) and 11–27 m during NF1802 (C4-C5).

$NO_3^- + NO_2^-$, ammonium, phosphate and DON concentrations

The concentrations of $NO_3^- +$ nitrite ($NO_3^- + NO_2^-$) in water-column samples were measured using a chemiluminescent method with a lower quantification limit of 0.1 μM and mean standard deviation of ±0.1 μM (Braman & Hendrix, 1989). Concentrations of NH_4^+ were quantified using the fluorescent OPA method with a lower limit of 25 nM and mean standard deviation of ±20 nM (Holmes *et al.*, 1999). Soluble reactive phosphorus (PO_4^{3-}) concentration measurements were made using colorimetric methods with a lower quantification limit of 50 nM (Koroleff, 1983). Concentrations of total dissolved nitrogen (TDN) were measured using persulfate oxidation of TDN to NO_3^- according to (Knapp *et al.*, 2005), and the resulting NO_3^- concentration was measured using chemiluminescence as described above. The concentration of DON was calculated by subtracting the concentrations of $NO_3^- + NO_2^-$ and NH_4^+ from the TDN concentration. In samples with undetectable levels of $NO_3^- + NO_2^-$ (i.e. most samples in the upper 100 m), the average standard deviation of DON concentration was ±0.3 μM, with a propagated error for DON concentration with detectable levels of $NO_3^- + NO_2^-$ of ±0.32 μM.

$NO_3^- + NO_2^-$ $\delta^{15}N$, $\delta^{18}O$ and DON $\delta^{15}N$ measurements

The $\delta^{15}N$ of $NO_3^- + NO_2^-$ in samples was measured using the denitrifier method (Casciotti *et al.*, 2002, Sigman *et al.*, 2001, Weigand *et al.*, 2016) and calibrated using standard bracketing techniques with IAEA N3 ($\delta^{15}N = 4.7‰$, $\delta^{18}O = 25.6‰$), and USGS 34 ($\delta^{15}N = -1.8‰$, $\delta^{18}O = -27.9‰$), and for $\delta^{18}O$, additionally with USGS 35 ($\delta^{18}O = 57.5‰$) as described by (Mcilvin & Casciotti, 2011). The mean standard deviation of replicate $NO_3^- + NO_2^-$ $\delta^{15}N$ and $\delta^{18}O$ analyses was <0.2‰. The $\delta^{15}N$ of TDN was determined using persulfate oxidation according to (Knapp *et al.*, 2005), with the resulting NO_3^- $\delta^{15}N$ determined with the denitrifier method after adjusting the sample to pH = 4. The $\delta^{15}N$ of DON was calculated by mass balance by subtracting the concentration and $\delta^{15}N$ of $NO_3^- + NO_2^-$ from the TDN concentration and $\delta^{15}N$. When the concentration of $NO_3^- + NO_2^-$ was below detection, the average standard deviation of duplicate analyses of DON $\delta^{15}N$ was ±0.3‰. When the concentration of $NO_3^- + NO_2^-$ was proportionate to the concentration of DON in the sample the propagated error for replicate analyses of DON $\delta^{15}N$ was ±0.6‰, determined using a Monte Carlo approach (Press *et al.*, 1992).

Chlorophyll *a* concentration, *Trichodesmium* spp. abundance, and suspended particulate N concentration and $\delta^{15}N$ measurements

The concentration of chlorophyll *a* was determined by calibrating the CTD fluorescence sensor with Niskin-bottle based HPLC pigments as described in Selph *et al.* (2021). Additionally, trichomes of the diazotroph *Trichodesmium* spp. were enumerated digitally using an OMAX A355OU camera and ToupLite software as described in (Selph *et al.*, 2021). Suspended particulate organic nitrogen (PN_{susp}) was collected by filtering 2.2 L of water onto a precombusted (450°C for 4 h) Whatman glass fiber filter and its mass and isotopic composition was determined by an elemental analyzer interfaced to an isotope ratio mass spectrometer at the UC Davis Stable Isotope Facility with a lower detection limit of 2.2 μg N and precision of ±0.3‰ for 80 μg N samples.

Sinking particulate N flux and $\delta^{15}N$ measurements

Surface-tethered, VERTEX-style particle-interceptor traps (PIT) were deployed at three depths: a "shallow" trap deployed at 60 m, below the mixed layer; a "mid-depth" trap deployed just below the base of the euphotic

zone (i.e. 117 m on C5, 140 m on C1-C3, and 151 m on C4); and a "deep" trap deployed at 231 m. PIT tubes (8:1 aspect ratio, baffle on top constructed of smaller tubes with 8:1 aspect ratio) were deployed with a formalin-brine for 2.2–4.5 days. After recovery, they were filtered through a 100-μm filter and swimmers were removed during inspection at 25× magnification (Zeiss stereomicroscope). Triplicate brine tubes were then filtered through precombusted Whatman glass fiber filters and the N mass flux ("PN_{sink} flux") and $\delta^{15}N$ of the PN_{sink} flux were determined as described above for suspended particles. A complete description of the sediment trap deployment and sample collection is given in (Stukel *et al.*, 2021).

Zooplankton excretion flux and its isotopic composition

Estimates of N loss from the euphotic zone due to excretion of diel migrant zooplankton at their mesopelagic daytime depths were calculated from the size-fractioned biomass measurements of (Landry & Swalethorp, 2021) and the empirical allometric relationship of Ikeda (1985) for ammonium and/or urea excretion (E: μg N organism^{-1} h^{-1}):

$$\ln E = -2.176 + 0.829 \ln C_i + 0.0648T$$

where C_i is the average C content of individual zooplankters in size fraction *i* and T (°C) is the environmental temperature at 300–500 m. Mesozooplankton were collected daily during experimental cycles at mid-day and mid-night with a 1-m diameter ring net (0.2-mm Nitex mesh) towed obliquely through the euphotic zone. The collected organisms were wet sieved through nested Nitex screens of 5, 2, 1, 0.5 and 0.2 mm Nitex mesh to produce five size classes of 0.2–0.5, 0.5–1, 1–2, 2–5 and >5 mm. Size fractions were oven dried (60°C) for total dry weight, ground to a powder, and analyzed for C and N content and isotopes ($\delta^{13}C$ and $\delta^{15}N$) by an elemental analyzer coupled to an isotope ratio mass spectrometer (EA-IRMS) (Owens and Rees, 1989). For each pair of day–night samples, migrant biomass was determined as the difference between night–day C for each size fraction. For individual C contents, C_i, in the Ikeda (1985) equation, we used mean values of 2.4, 7.4, 41, 140 and 2 782 μg C ind^{-1} for the 0.2–0.5 to >5 mm size fractions, respectively (Landry *et al.*, 2001). Migrant abundances in each size fraction were calculated from measured C biomass and the individual C_i estimates, and migrants were assumed to spend 12 h d^{-1} at mesopelagic depths (300–500 m).

Since few have measured it directly, we consider the $\delta^{15}N$ of zooplankton excretion to be relatively uncertain. Consequently, we used lower and upper bound estimates, 3‰ and 5‰, respectively, for the magnitude of the isotope effect associated with zooplankton N excretion. The 3‰ estimate reflects the difference between the $\delta^{15}N$ of copepod and doliolid biomass and excreted N in the northwest Pacific Ocean (Checkley & Miller, 1989). This estimate is also consistent with prior studies of N isotopic enrichment in food webs (Checkley & Entzeroth, 1985, Deniro & Epstein, 1981, Minagawa & Wada, 1984, Wada *et al.*, 1987). The 5‰ estimate comes from organismal N mass and isotopic observational and modeling constraints (Stukel *et al.*, 2018). Uncertainties in the day–night biomass of each size class were propagated through all measurements using Monte Carlo approaches.

RESULTS

$NO_3^- + NO_2^-$ concentration, $\delta^{15}N$, $\delta^{18}O$

The concentration of $NO_3^- + NO_2^-$ in the upper 100 m was <0.1 μM and increased with depth (Figs. 2 and 3). Water-column profiles of thermocline $NO_3^- + NO_2^-$ $\delta^{15}N$ and $\delta^{18}O$ show similar trends among the cycles and little variation on potential density surfaces, with a $NO_3^- + NO_2^-$ $\delta^{15}N$ maximum of ∼5‰ at 650 m, which decreases up through the shallower thermocline to a minimum of 2.0 to 3.0‰ at 231 m (Figs. 2 and 3). The $\delta^{18}O$ of $NO_3^- + NO_2^-$ throughout the water column was largely 1.5 ± 0.5‰ (Fig. 3), with the $\delta^{18}O$ of $NO_3^- + NO_2^-$ in samples shallower than 150 m > 3.0‰ in the same samples with elevated $NO_3^- + NO_2^-$ $\delta^{15}N$ (Fig. 3).

DON and PN_{susp} concentration and $\delta^{15}N$

DON concentration in the NF1802 samples was largely consistent among stations (Fig. 4). Profile concentrations averaged between 4 and 5 μM in the upper 100 m. The mean $\delta^{15}N$ of DON varied between 3.0 and 3.5‰, but showed more variability among stations than DON concentration (Figs. 4 and 5). Exceptions to these mean values include a station from C5 near the shelf/slope break where higher DON concentration (7.3 μM) was found in surface waters with a relatively elevated $\delta^{15}N$ of 4.5‰ (Fig. 4). This surface water sample also had a relatively low salinity (35.28) compared with the underlying 40 m sample (36.45). However, other samples further offshore with a similar salinity, 35.0–36.0, had a $\delta^{15}N$ between 3.0 and 4.0‰ (Fig. 4). Other samples

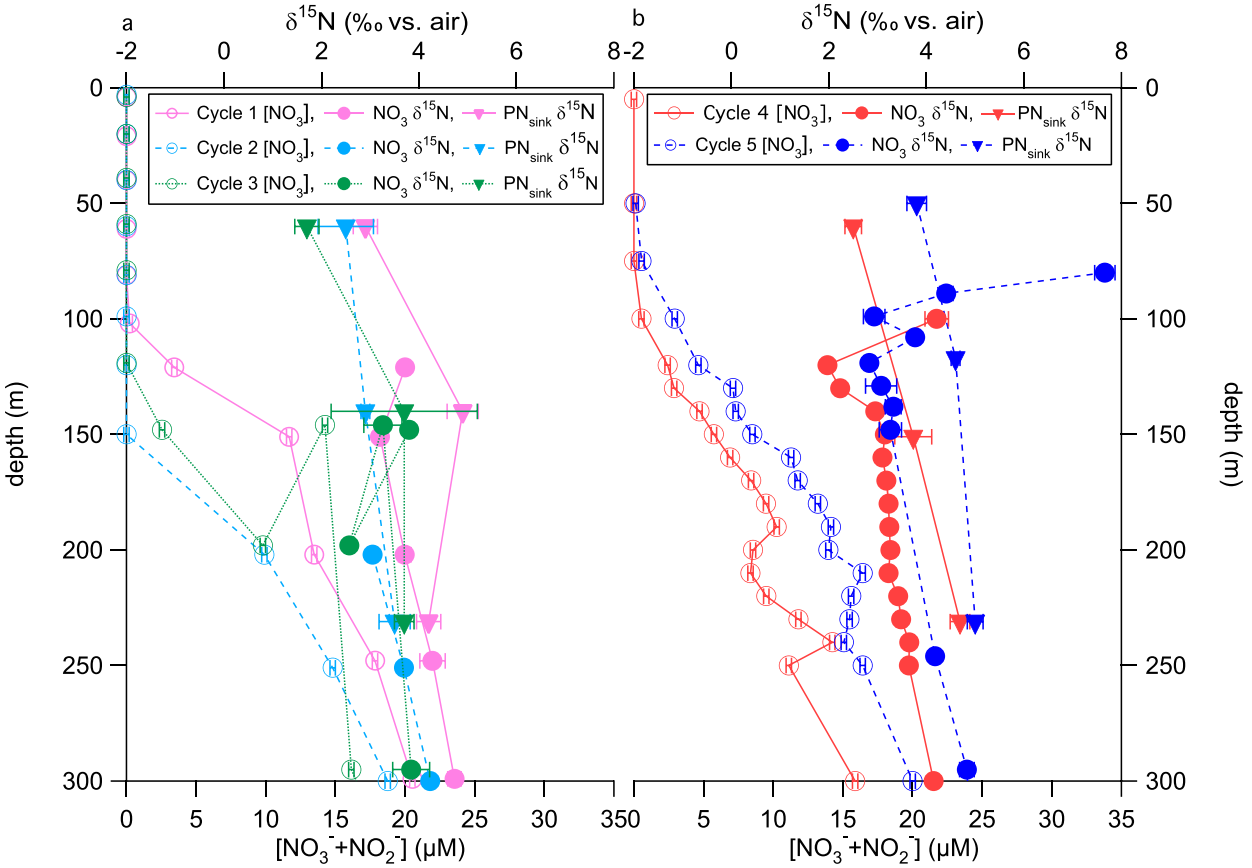

Fig. 2. Measurements supporting $\delta^{15}N$ budget calculations, including the concentration (open circles) and $\delta^{15}N$ (filled circles) of $NO_3^- + NO_2^-$ as well as PN_{sink} $\delta^{15}N$ (filled triangles) from the 2017 (a) and 2018 (b) cruises, with "C1" represented by solid pink lines, "C2" represented by dashed light blue lines, "C3" represented by dotted green lines, "C4" represented by solid red lines, and "C5" represented by dashed dark blue lines. Error bars represent ±1 S.D. and are smaller than the symbol size for $NO_3^- + NO_2^-$ concentration and often the $NO_3^- + NO_2^-$ $\delta^{15}N$ measurements.

near the shelf/slope break collected from 75 and 100 m with relatively high DON $\delta^{15}N$, from 4.0 to 6.0‰, had salinities >36. Additionally, two stations further offshore had $\delta^{15}N$ DON <3‰ at several depths in the upper 100 m (Fig. 4). All samples at these stations had salinity >36. No significant changes in DON concentration or $\delta^{15}N$ were found over the course of the Lagrangian cycles (Figs. 4 and 5).

The mean PN_{susp} concentration in the upper 100 m on the NF1704 cruise was ~1.0 μM, and ranged from 0.7 to 2.0 μM and was higher than the mean PN_{susp} concentration on the NF1802 cruise (mean ~ 0.6 μM, ranging from 0.3 to 1.3 μM) (Fig. 5) (Table III). The mean $\delta^{15}N$ of PN_{susp} on NF1704, 1.0–2.0‰, was not significantly different from that on NF1802, 1.0–2.5‰. Finally, like DON, we found no significant gradients with depth or over the course of the Lagrangian cycles for either PN_{susp} concentration or $\delta^{15}N$ in the upper 100 m (Fig. 5) (Table III).

The flux and isotopic composition of PN_{sink} and zooplankton excretion

The largest flux of N out of the euphotic zone was the PN_{sink} flux. The range and mean PN_{sink} mass flux (±1 SD) and mean, mass-weighted $\delta^{15}N$ of the PN_{sink} flux (±1 S.D.) for each cycle, determined by averaging the PN_{sink} collected in three brine tubes per floating sediment trap deployment, is reported in Table I (Fig. 2). The mean PN_{sink} mass flux into the 60 m traps, representing upper euphotic zone export from the mixed layer, ranged from 0.59 ± 0.04 (C4) to 1.53 ± 0.6 (C1) mmol N m^{-2} d^{-1} (Table I). Mean PN_{sink} fluxes out of the euphotic zone, as recorded by the mid-depth trap, ranged from 0.46 ± 0.02 (C1) to 1.1 ± 0.18 (C3) mmol N m^{-2} d^{-1} (Table I). The mean PN_{sink} mass flux decreased with depth except for C3, when the PN_{sink} flux in the 140 m trap was larger than (although not significantly different from) that captured in the 60 m trap, 1.1 ± 0.18 vs. 0.98 ± 0.26 mmol N m^{-2} d^{-1}, respectively (Table I). The

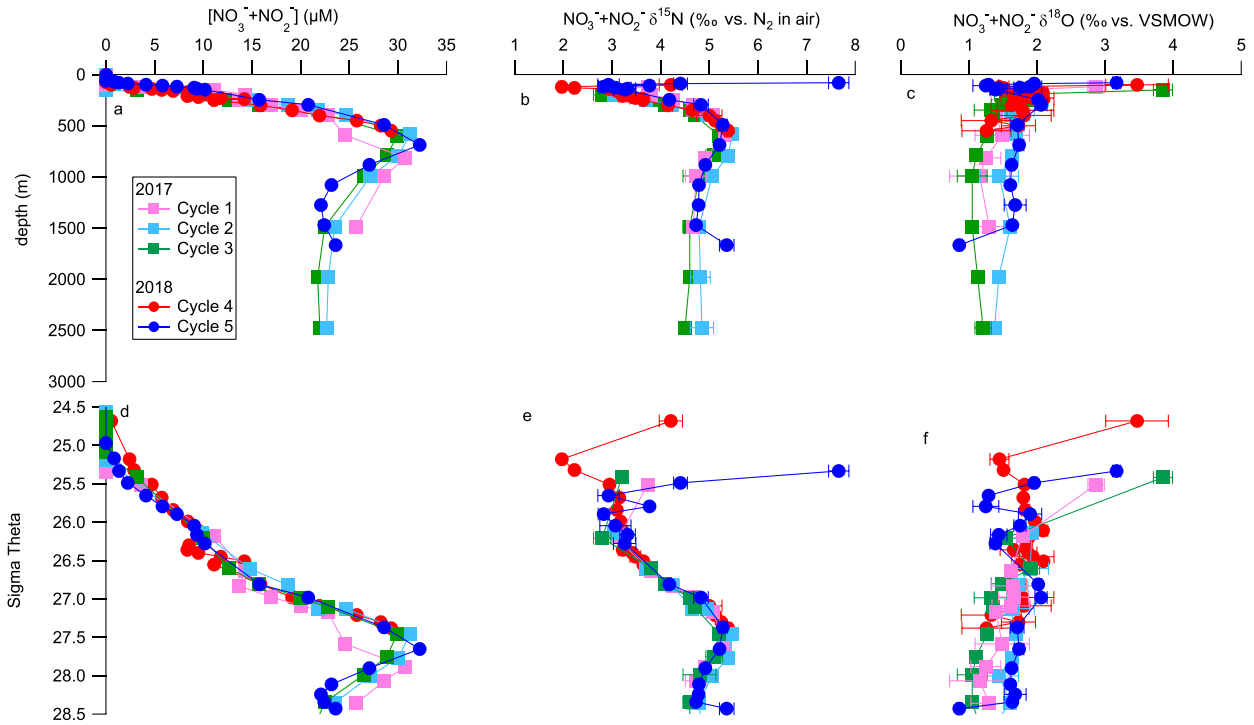

Fig. 3. The concentration, $\delta^{15}N$, and $\delta^{18}O$ of $NO_3^- + NO_2^-$ from the NF1704 (filled squares) and NF1802 (filled circles) cruises plotted vs. depth (a, b, and c, respectively) and on sigma theta surfaces (d, e, and f, respectively). Error bars represent ±1 S.D. and are smaller than the symbol size for $NO_3^- + NO_2^-$ concentration. Colors follow from Fig. 2.

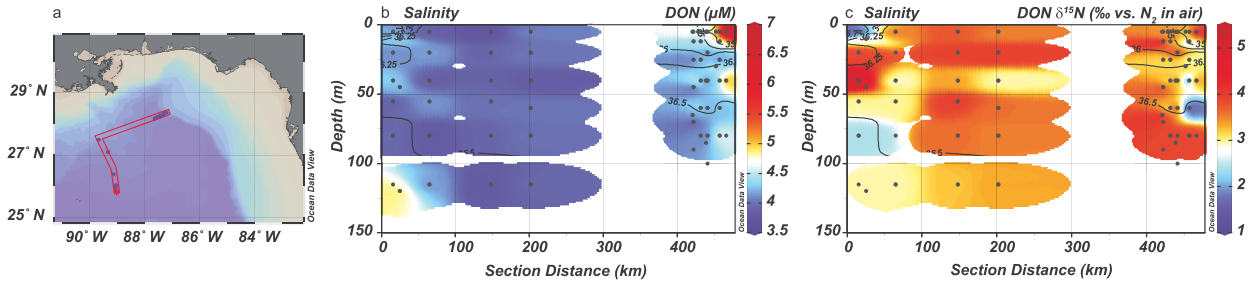

Fig. 4. Location of sampling during the 2018 cruise (a) with concentration (b) and $\delta^{15}N$ (c) of DON in the upper 150 m. Cross-section begins at southwest end and finishes at northeast end of transect. Salinity contours overlay DON concentration and $\delta^{15}N$ color contours in panels (b) and (c), respectively.

PN_{sink} flux in the 231 m trap was 35–50% of the PN_{sink} flux at the base of the euphotic zone (Table I). The mean $\delta^{15}N$ of the PN_{sink} flux at 60 m, ranging from 1.6 ± 0.3‰ (C3) to 3.8 ± 0.2‰ (C5), was lower than the $\delta^{15}N$ of PN_{sink} flux in the deeper traps (Fig. 2, Table I). The $\delta^{15}N$ of the PN_{sink} flux in the deepest two traps were typically more similar to each other than the $\delta^{15}N$ of the PN_{sink} flux in the euphotic zone, and the mean $\delta^{15}N$ for both of the deeper traps ranged from 2.9 ± 0.1‰ (C2, 120 m) to 5.0 ± 0.2‰ (C5, 231 m) (Table I). Finally, we note that the $\delta^{15}N$ of the PN_{sink} flux was always higher than the $\delta^{15}N$ of PN_{susp}.

Since we observed no gradients either with depth or over the course of Lagrangian sampling in either PN_{susp} or DON concentration in the euphotic zone (Table III, Figs. 4 and 5), the only other quantifiable pathway for N loss from the euphotic zone is via excretion or defecation of nitrogenous waste from vertically migrating zooplankton at depth or mortality of these organisms at their daytime resting depths. The estimated rates of zooplankton N excretion, in the form of NH_4^+ (Checkley & Miller, 1989) and urea (Bidigare, 1983), below the euphotic zone are reported in Table II. The mean excretion rates of all vertically migrating

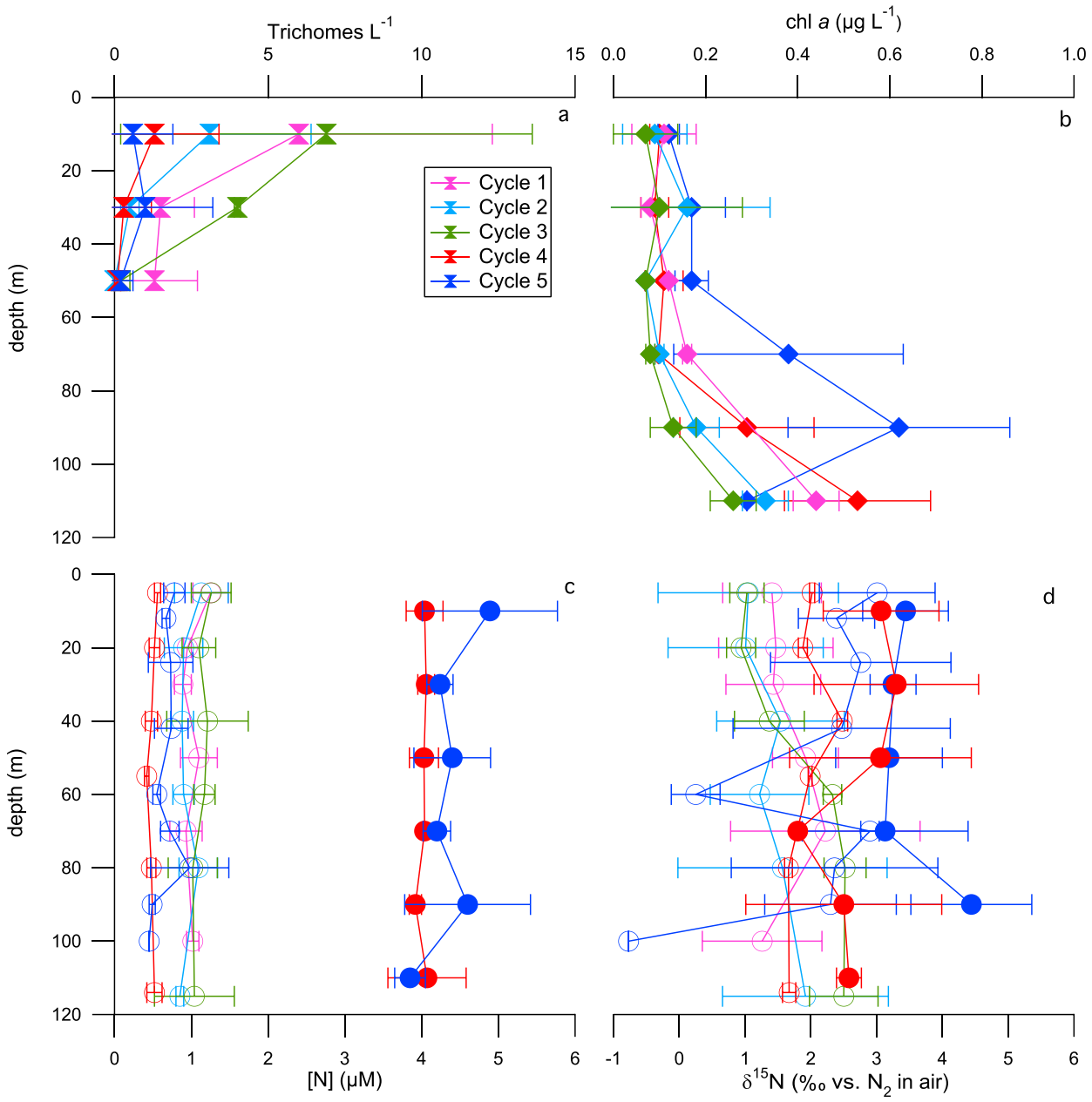

Fig. 5. Cycle-mean (±1 S.D., with cycle colors following from previous figures) upper water column *Trichodesmium* spp. trichome abundance (bow tie symbol) (a); chlorophyll *a* concentration (filled diamonds) (b), PN_{susp} concentration (open circles) and DON concentration (filled circles) (c), and PN_{susp} $\delta^{15}N$ (open circles) and DON $\delta^{15}N$ (filled circles) (d).

zooplankton size classes were summed for each cycle, and range from 19.6 ± 49.1 (C1) to 171.7 ± 103.3 (C5) µmol N m^{-2} d^{-1} (Table II), with detailed descriptions of these fluxes in (Landry & Swalethorp, 2021). These zooplankton excretion fluxes are roughly an order of magnitude smaller than the PN_{sink} fluxes below the euphotic zone (Tables I and II). Although we could not quantify zooplankton mortality or defecation at depth, we believe these fluxes are also small relative to PN_{sink} and hence neglect them in further calculations. Estimates of the $\delta^{15}N$ of zooplankton excretion assuming a 3‰ isotope effect range from 0.6 to 3.1‰ and are similar to or lower than the $\delta^{15}N$ of both subsurface $NO_3^- + NO_2^-$ and the PN_{sink} flux (Table I), which range from −0.8 to 1.7‰ using the 5‰ isotope effect (Table II).

Table I: The mass and isotopic composition of the sinking particulate nitrogen flux captured in drifting sediment traps, and results of $\delta^{15}N$ budgets for traps deployed below the base of the euphotic zone for 2017 and 2018 cruises, including the range in $NO_3^- + NO_2^-$ $\delta^{15}N$ end-member, fraction of export supported by N_2 fixation ("F_{N2fix}") and N_2 fixation rate determined by multiplying PN_{sink} flux by F_{N2fix}. The fractional importance of N_2 fixation and geochemical N_2 fixation rate estimates include contributions from zooplankton excretion at depth (Table II), see text for details.

Year	Cycle	Trap depth (m)	Mass flux range (mmol N m^{-2} d^{-1})	Mean mass flux (± 1 SD) (mmol N m^{-2} d^{-1})	PN_{sink} $\delta^{15}N$ range (‰ vs. N_2 in air)	Mean PN_{sink} $\delta^{15}N$ (± 1 SD) (‰ vs. N_2 in air)	$NO_3^- + NO_2^-$ $\delta^{15}N$ (‰ vs. N_2 in air)	F_{N2fix} (%)	N_2 fix rate (μmol N m^{-2} d^{-1})
2017	1	60	1.01–2.10	1.53 ± 0.6	2.7–3.2	2.9 ± 0.3			
		140	0.44–0.49	0.46 ± 0.02	4.5–5.1	4.9 ± 0.3	3.2–3.8‰	0	0
		231	0.17–0.20	0.19 ± 0.02	4.1–4.5	4.2 ± 0.3			
	2	60	0.79–0.88	0.82 ± 0.05	1.9–2.9	2.5 ± 0.6			
		140	0.38–0.72	0.52 ± 0.18	2.8–2.9	2.9 ± 0.1	3.1–3.7‰	18 ± 8	90 ± 40
		231	0.19–0.25	0.22 ± 0.03	3.3–3.9	3.6 ± 0.3			
	3	60	0.83–1.28	0.98 ± 0.26	1.4–1.8	1.6 ± 0.3			
		140	1.01–1.34	1.1 ± 0.18	1.0–1.3	3.9 ± 1.5	2.8–3.8‰	0 ± 30	0 ± 336
		231	0.32–0.55	0.4 ± 0.13	3.5–3.9	3.6 ± 0.2			
2018	4	60	0.45–0.62	0.59 ± 0.04	2.4–2.7	2.5 ± 0.2			
		151	0.38–0.57	0.47 ± 0.10	3.4–3.7	3.8 ± 0.4	2.0–2.2‰	0	0
		231	0.23–0.25	0.25 ± 0.01	4.5–4.9	4.7 ± 0.2			
	5	60	1.00–1.13	1.08 ± 0.07	3.6–4.0	3.8 ± 0.2			
		117	0.67–1.03	0.87 ± 0.18	4.5–4.7	4.6 ± 0.1	2.9–3.8‰	0	0
		231	0.30–0.34	0.32 ± 0.02	4.8–5.1	5.0 ± 0.2			

Table II: The ammonia+urea excretion flux by diel vertically migrating zooplankton and its estimated isotopic composition. All zooplankton size fractions were summed and the bulk zooplankton isotopic composition represents the mass-weighted mean $\delta^{15}N$ of all zooplankton size fractions in each cycle. The estimated $\delta^{15}N$ of the excretion flux is calculated by: 1) assuming a difference of 3‰ between the $\delta^{15}N$ of the bulk zooplankton biomass and the $\delta^{15}N$ of the excretion (next to last column) (Checkley and Miller, 1989), and, 2) modeling zooplankton size and fraction of biomass below the euphotic zone, and assuming an isotope effect of 5‰ for zooplankton excretion (last column) (Stukel et al., 2018). See text for details.

Year	Cycle	Export depth (m)	Net tows (n)	Mass flux range (μmol N m^{-2} d^{-1})	Mean mass Flux (± 1 SD) (μmol N m^{-2} d^{-1})	ZP $\delta^{15}N$ (± 1 SD) (‰ vs. N_2 in air)	Excreted $\delta^{15}N$* (±1 SD) (‰ vs. N_2 in air)	Excreted $\delta^{15}N$# (± error) (‰ vs. N_2 in air)
2017	1	100	7	−37.0 to 49.2	19.6 ± 49.5	6.0 ± 1.3	3.0 ± 1.3	1.7 ± 0.7
	2	100	4	49.0–119.8	84.4 ± 50.1	4.1 ± 1.2	1.1 ± 1.2	−1.8 ± 0.4
	3	100	8	−52.0 to 126.8	41.9 ± 85.5	4.1 ± 1.2	1.1 ± 1.2	−1.1 ± 0.4
2018	4	100	9	−69.5 to 138.5	37.7 ± 87.2	3.6 ± 1.4	0.6 ± 1.4	−1.1 ± 0.2
	5	100	9	81.9–309.0	171.7 ± 103.3	6.1 ± 1.0	3.1 ± 1.0	0.2 ± 0.3

[a]Estimated according to Checkley and Miller (1989), where $\delta^{15}N$ of excretion flux is 3‰ lower than the $\delta^{15}N$ of zooplankton.
[b]Estimated using a 5% isotope effect for zooplankton excretion as outlined in Stukel *et al.* (2018).

DISCUSSION

Comparison with prior regional observations

Water-column profiles of $NO_3^- + NO_2^-$ concentration and isotopic composition from these cruises were consistent with prior regional observations (Howe *et al.*, 2020). In particular, the decreasing $NO_3^- + NO_2^-$ $\delta^{15}N$ up through the thermocline (Fig. 3) has been observed previously in the GoM and North Atlantic and is consistent with prior characterizations of the isotopic composition of $NO_3^- + NO_2^-$ in regional water masses including the GoM (Howe *et al.*, 2020), the Florida Straits (Leichter *et al.*, 2007), and the North Atlantic (Knapp *et al.*, 2008, Marconi *et al.*, 2015, Marconi *et al.*, 2019). The increasing $\delta^{15}N$ and $\delta^{18}O$ of $NO_3^- + NO_2^-$ in the upper 150 m is consistent with NO_3^- assimilation at the base of the euphotic zone as has been observed

previously in the region (Howe *et al.*, 2020, Knapp *et al.*, 2005). The similarities of GoM samples to $NO_3^- + NO_2^-$ concentration, $\delta^{15}N$, and $\delta^{18}O$ from the North Atlantic are consistent with the Loop Current importing thermocline water from the tropical and subtropical North Atlantic into the GoM (Hernandez-Guerra & Joyce, 2000, Hofmann & Worley, 1986, Morrison *et al.*, 1983, Wilson & Johns, 1997), as well as the relatively short residence time of water in the GoM (Amon *et al.*, 2020). The latter prevents N inputs from the Mississippi River, submarine groundwater discharge, and N_2 fixation from significantly modifying the concentration and isotopic composition of $NO_3^- + NO_2^-$ before leaving the GoM (Howe *et al.*, 2020).

To the best of our knowledge, these measurements of DON $\delta^{15}N$ are the first reported from the GoM. As was found for the concentration and isotopic composition of $NO_3^- + NO_2^-$, these DON observations are consistent with regional observations from the Sargasso Sea, between 3.0 and 4.0‰ (Figs. 4 and 5) (Knapp *et al.*, 2005, Knapp *et al.*, 2011). The sample from C5 near the shelf/slope break with elevated DON concentration and $\delta^{15}N$ and slightly lower salinity was collected near DeSoto Canyon, and it is possible that the surface sample included freshwater DON, possibly from the Mississippi-Atchafalaya River System, other riverine (e.g. Apalachicola) inputs, benthic DON, and/or submarine groundwater discharge (Morey *et al.*, 2003). Alternatively, the elevated concentration and isotopic composition may reflect production of DON near the shelf/slope break (Kelly *et al.*, 2021) that underwent subsequent consumption with isotopic fractionation (Knapp *et al.*, 2018a, Zhang *et al.*, 2020). Other samples collected near the shelf/slope break with elevated DON $\delta^{15}N$ values deeper in the water column are not associated with a decrease in DON concentration between the surface and subsurface, indicating a different DON source and not remineralization with depth as a likely explanation with benthic sources potentially including submarine groundwater discharge (Sanial *et al.*, 2021). A distinct DON source, such as benthic organic matter and/or submarine groundwater discharge, may also be responsible for the low-$\delta^{15}N$ DON (1.7‰) observed near De Soto Canyon (Fig. 4).

While 100 m samples collected offshore with relatively low DON $\delta^{15}N$ (<3‰) and salinity >36 were not associated with elevated *Trichodesmium* spp. trichome abundance, they may reflect recent low-$\delta^{15}N$ inputs not captured by *Trichodesmium* spp. abundance at the time of sampling. It is also notable that although *Trichodesmium* spp. were most abundant in the upper 20 m (Fig. 5) (Selph *et al.*, 2021), consistent with prior observations of their depth distribution (Capone *et al.*, 2005), the $\delta^{15}N$ of DON was not significantly lower in the upper 20 m than throughout the upper 100 m (Figs. 4 and 5). Thus, if DON was released by *Trichodesmium* spp., it did not accumulate to detectable levels in this pool (Knapp *et al.*, 2011), but instead may have been assimilated by other phytoplankton that could then contribute to the sinking flux (e.g. (Bonnet *et al.*, 2016, Knapp *et al.*, 2016b)). We note that *Trichodesmium* spp. trichome abundance was low compared to prior work in the Atlantic, where an average of >2000 trichomes L^{-1} was observed (Carpenter *et al.*, 2004). No significant trends in DON concentration or $\delta^{15}N$ with depth were observed, which is also consistent with losses of DON not typically observed in the upper 100 m in oligotrophic regions, but instead seen at or below 150 m (Knapp *et al.*, 2011). Finally, there is no evidence for differences in DON concentration in the upper 50 m vs. the 50–100 m depth horizon (Figs. 4 and 5), as would be consistent with DON consumption within the euphotic zone observed in regions transitional between productive and oligotrophic regions (Knapp *et al.*, 2018a, Zhang *et al.*, 2020).

The mean PN_{susp} concentration on these cruises, in particular on the NF1704 cruise, was higher than is typically found in oligotrophic environments such as Bermuda and Hawaii. The concentrations of PN_{susp} on NF1802 were closer to those typically observed in oligotrophic euphotic zones such as near Hawaii and Bermuda, where PN_{susp} concentrations are typically 0.3–0.4 μM (Altabet, 1988, Fujiki *et al.*, 2011). It is not clear why the PN_{susp} was twice as high on NF1704 compared to NF1802, as chlorophyll *a* concentrations in the upper 50 m were not meaningfully different between the 2 years (Fig. 5), nor were other productivity metrics (Yingling *et al.*, 2021). The similarity of the mean $\delta^{15}N$ of PN_{susp} on both cruises suggests similar N supply and cycling mechanisms were at work during both cruises. Regardless, the $\delta^{15}N$ of this PN_{susp} was higher than that typically observed in the Sargasso Sea, −1 to 0‰ (Altabet, 1988, Fawcett *et al.*, 2011), or in other tropical Atlantic regions where diazotrophs are abundant (Montoya *et al.*, 2002).

The PN_{sink} mass fluxes captured in the subeuphotic zone traps are somewhat lower than observations closer to the northern GoM shelf/slope break region (Hung *et al.*, 2004; Hung *et al.*, 2010), but similar to other observations from the Gulf from deeper waters (Maiti *et al.*, 2016). Additionally, these PN_{sink} fluxes are similar to results from the Sargasso Sea (Altabet, 1988) and are somewhat higher than fluxes in the oligotrophic North (Casciotti *et al.*, 2008, Christian *et al.*, 1997) and South Pacific (Knapp *et al.*, 2016a). Finally, the elevation of the $\delta^{15}N$ of the PN_{sink} flux relative to the $\delta^{15}N$ of PN_{susp} is consistent with prior observations (Altabet, 1988, Altabet *et al.*, 1991, White *et al.*, 2013).

δ^{15}N budget constraints on the sources of N fueling export production in the GoM

In spite of low inorganic nutrient concentrations, oligotrophic surface waters still support rates of export production comparable to regions with higher surface nutrient concentrations (Emerson, 2014). Older δ^{15}N budgets in a similarly stratified oligotrophic region near Hawaii have suggested that N_2 fixation provides as much as 50% of the N supporting export production (Karl *et al.*, 1997; Dore *et al.*, 2002). However, more recent δ^{15}N budgets, employing sensitive methods to measure the δ^{15}N of NO_3^- present at lower concentrations immediately below the euphotic zone indicate that export production is primarily fueled by NO_3^- near Hawaii (Casciotti *et al.*, 2008), assuming that the PN_{sink} flux is the primary N loss pathway from the euphotic zone. Even though PN_{sink} is the largest flux of N out of the euphotic zone, zooplankton vertical migration and mortality or N excretion at depth and vertical mixing of DOM and/or POM can also be an important vector for C and N loss from surface waters (Emerson, 2014) (Fig. 6). In the Sargasso Sea near Bermuda, previous δ^{15}N budgets have considered the potential importance of DON and PN_{susp} consumption as a N source fueling export production (Knapp *et al.*, 2005). In this previous study, with DON concentration and δ^{15}N similar to those in the GoM, calculated DON and PN_{susp} consumption did not play a quantitatively important role supporting export (Knapp *et al.*, 2005). Since a stably stratified water column suggested weak mixing and DON and PN_{susp} vertical gradients were not pronounced (Table III, Figs. 4 and 5), and since no significant gradients were observed over the duration of the Lagrangian cycles either, we cannot include PN_{susp} or DON in these δ^{15}N budget calculations. However, we note that consumption of either PN_{susp} or DON at rates sufficient to support the magnitude of export production observed in the mid-depth trap would be difficult to resolve in these measurements. For instance, if the PN_{sink} flux in the subeuphotic trap of C1, 0.46 mmol N m^{-2} d^{-1} (Table I) was entirely supported by the consumption of DON or PN_{susp} occurring equally throughout the upper 100 m, it would correspond to a loss of 4.6 nM N d^{-1} from the DON or PN_{susp} pool, not detectable in these concentration measurements over the course of the 2–4-day cycles.

With the exception of a recent study (Stukel *et al.*, 2018), previous δ^{15}N budgets have not quantified zooplankton N excretion at depth as another N loss term. Here, we include zooplankton excretion below the euphotic zone with the PN_{sink} flux in Eqn. 1 to estimate the δ^{15}N of total N loss from the euphotic zone and compare that with the δ^{15}N of the presumed largest source of N fueling export, subsurface NO_3^-; Fig. 6 illustrates this conceptually and includes the δ^{15}N of N pools and fluxes in this study. If the δ^{15}N of the combined, mass-weighted N loss terms is lower than the δ^{15}N of subsurface NO_3^- it implies that the δ^{15}N budget is imbalanced and an additional source of N to the euphotic zone with a lower δ^{15}N is required to balance the isotopic composition of N losses. Here, we assume N_2 fixation is the best candidate for that low-δ^{15}N N source, which introduces N with a δ^{15}N between −2 and 0‰ to the euphotic zone (Carpenter *et al.*, 1997, Hoering & Ford, 1960, Minagawa & Wada, 1986). However, we note that atmospheric deposition of N has a similarly low δ^{15}N signature (Dillon & Chanton, 2005, Hastings *et al.*, 2003, Knapp *et al.*, 2010).

First considering the δ^{15}N of the source NO_3^-, we see that water-column samples collected shallower than 231 m show elevation in $NO_3^- + NO_2^-$ δ^{15}N and δ^{18}O as the $NO_3^- + NO_2^-$ concentration decreases (Figs. 2 and 3). This increase in both the δ^{15}N and δ^{18}O of $NO_3^- + NO_2^-$ reflects NO_3^- assimilation, as is commonly observed below the euphotic zone (Granger *et al.*, 2004, Knapp *et al.*, 2008, Wankel *et al.*, 2007), and thus does not represent the δ^{15}N of the source NO_3^-. Given the difficulty in identifying the precise $NO_3^- + NO_2^-$ source depth, we evaluate a range in $NO_3^- + NO_2^-$ δ^{15}N end-members, including the shallow $NO_3^- + NO_2^-$ δ^{15}N minima in each profile, as well as the $NO_3^- + NO_2^-$ δ^{15}N in the sample collected immediately below the δ^{15}N minima, in the δ^{15}N budget calculations (Eqn. 1) (Table I). Using a range of $NO_3^- + NO_2^-$ δ^{15}N values for the end-member when calculating the importance and rate of N_2 fixation allows for variability in the depth from which $NO_3^- + NO_2^-$ is being mixed into the euphotic zone via, e.g. internal waves breaking near the continental shelf (Sharples *et al.*, 2009, Sharples *et al.*, 2007) and/or eddy pumping (Falkowski *et al.*, 1991).

Next, we consider the mass flux and isotopic composition of N loss pathways from the euphotic zone. The two loss terms included in the δ^{15}N budget calculations are the PN_{sink} flux and zooplankton excretion. As described above, the PN_{sink} flux is roughly an order of magnitude larger than the zooplankton excretion flux (Tables I and II, Fig. 6). Because the δ^{15}N of zooplankton excretion is lower than the δ^{15}N of the PN_{sink} flux, the δ^{15}N of the combined export fluxes is close to, but up to 0.3‰ lower than, the δ^{15}N of the PN_{sink} flux. Including the mass-weighted δ^{15}N of the zooplankton excretion flux estimated according to Checkley and Miller (1989) (Table II) together with the PN_{sink} flux modifies the δ^{15}N of the combined flux most significantly for C2, where it increases the importance of N_2 fixation from supporting ∼10 to 18% of export production. When evaluating the δ^{15}N budgets, we include both the range in the δ^{15}N of

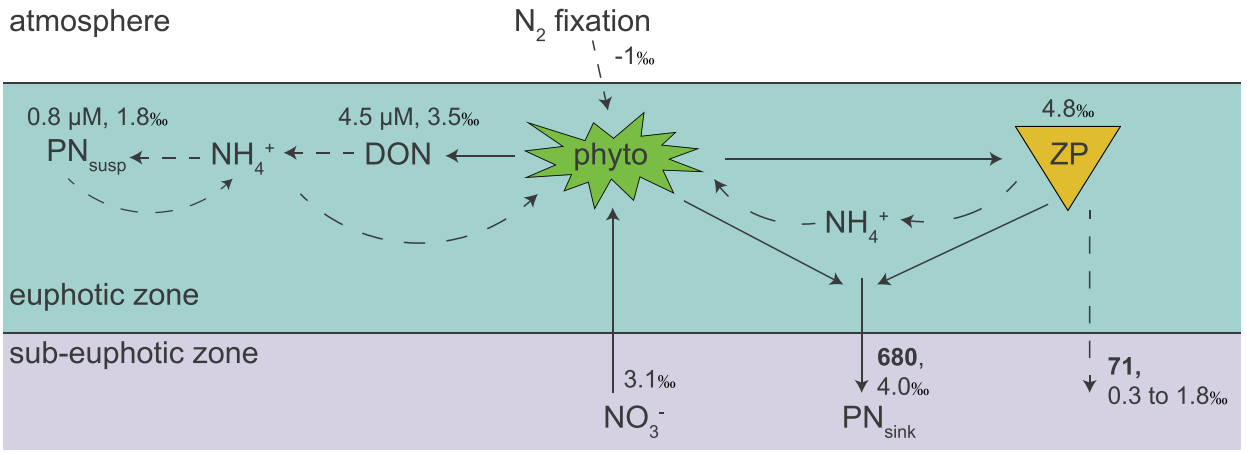

Fig. 6. Schematic of nitrogen pools and fluxes to, from, and within the euphotic zone in the oligotrophic Gulf of Mexico. Dashed lines represent low-δ^{15}N fluxes, with solid lines representing transfers of relatively high δ^{15}N. The mean flux magnitudes for fluxes out of the euphotic zone quantified in this study, PN_{sink} and zooplankton excretion, are shown in bold, with units of µmol N m^{-2} d^{-1}, as well as their representative isotopic composition. The mean concentrations and δ^{15}N of PN_{susp} and DON in the euphotic are reported with concentration in units of µM. The δ^{15}N budgets described in the text compare the δ^{15}N of subsurface NO_3^- with the δ^{15}N of the PN_{sink} flux and the estimate of zooplankton excretion below the euphotic zone. Regenerated NH_4^+ represents an important low-δ^{15}N N source fueling phytoplankton in the euphotic zone.

Table III: Mean concentration and nitrogen isotopic composition of suspended particulate organic nitrogen (PN_{susp}) ± 1 SD

Cycle	Depth	PN_{susp} (µM) (±1 SD)	PN_{susp} δ^{15}N (±1 SD)	*n*
1	5	1.25 ± 0.23	1.41 ± 0.75	4
1	20	0.95 ± 0.05	1.47 ± 0.87	4
1	30	0.89 ± 0.11	1.43 ± 0.72	4
1	50	1.10 ± 0.24	1.92 ± 0.50	4
1	70	0.93 ± 0.21	2.22 ± 1.44	4
1	100	1.02 ± 0.08	1.26 ± 0.91	4
2	5	1.13 ± 0.35	1.05 ± 1.37	3
2	20	0.90 ± 0.25	1.01 ± 1.18	3
2	40	0.88 ± 0.15	1.54 ± 0.97	3
2	60	0.90 ± 0.14	1.22 ± 0.75	3
2	80	1.09 ± 0.25	1.57 ± 1.59	3
2	115	0.85 ± 0.05	1.92 ± 1.26	3
3	5	1.26 ± 0.26	1.03 ± 0.49	4
3	20	1.10 ± 0.22	0.94 ± 1.27	4
3	40	1.21 ± 0.53	1.37 ± 0.31	4
3	60	1.17 ± 0.14	2.33 ± 0.75	4
3	80	1.02 ± 0.32	2.52 ± 1.75	4
3	115	1.04 ± 0.52	2.50 ± 0.72	4
4	5	0.56 ± 0.04	2.02 ± 2.33	5
4	20	0.52 ± 0.07	1.88 ± 1.90	5
4	40	0.48 ± 0.08	2.48 ± 2.45	5
4	55	0.42 ± 0.03	1.99 ± 1.40	5
4	80	0.48 ± 0.06	1.66 ± 1.95	5
4	114	0.52 ± 0.10	1.67 ± 2.41	5
5	5	0.78 ± 0.14	3.01 ± 0.88	5
5	12	0.67 ± 0.05	2.39 ± 0.58	4
5	24	0.73 ± 0.29	2.76 ± 1.37	5
5	42	0.74 ± 0.22	2.47 ± 1.65	5
5	60	0.55 ± 0.05	0.25 ± 0.37	3
5	70	0.72 ± 0.12	2.90 ± 0.14	2
5	80	0.98 ± 0.51	2.36 ± 1.57	2
5	90	0.49 ± 0.04	2.30 ± 1.0	2
5	100	0.45	−0.77	1

the $NO_3^- + NO_2^-$ end-member as well as the standard deviation associated with the PN_{sink} $\delta^{15}N$ measurement in our uncertainty estimates (Table I).

Using these constraints in Eqn. 2 indicates that N_2 fixation was not detected as a N source supporting export production in four of the five cycles (Table I). This is qualitatively evident from comparing the $\delta^{15}N$ of the dominant N loss term, the PN_{sink} flux, with the $\delta^{15}N$ of subsurface $NO_3^- + NO_2^-$ (Fig. 2), and is consistent with the low abundance of *Trichodesmium* spp. in this study, <10 trichomes L^{-1} (Fig. 5) (Selph *et al.*, 2021) compared with prior work where >2000 trichomes L^{-1} have been observed in the tropical North Atlantic, e.g. (Capone *et al.*, 1998, Capone *et al.*, 1997, Carpenter *et al.*, 2004). We see that the $\delta^{15}N$ of the PN_{sink} + zooplankton excretion fluxes is nearly always higher than the $\delta^{15}N$ of subsurface $NO_3^- + NO_2^-$ (Fig. 2, Tables I and II). Only in C2 during the 2017 cruise was the $\delta^{15}N$ of the combined export fluxes lower than the $\delta^{15}N$ of subsurface $NO_3^- + NO_2^-$ (i.e. 2.6‰ vs. 3.1–3.7‰, respectively) (Fig. 2; Table I), allowing for an input from a low-$\delta^{15}N$ N source to balance the $\delta^{15}N$ of N inputs to and loss from the euphotic zone. N_2 fixation is estimated to have supported 18 ± 8% of export production during C2 (Table I). Multiplying this fractional importance of N_2 fixation by the combined PN_{sink} and zooplankton excretion fluxes yields an estimated N_2 fixation rate of 90 ± 40 μmol N m^{-2} d^{-1} during C2 (Table I). Additionally, the range in the $\delta^{15}N$ of subsurface $NO_3^- + NO_2^-$, the large standard deviation associated with the PN_{sink} $\delta^{15}N$ measurement, and the high PN_{sink} flux indicates that N_2 fixation during C3 supported 0 ± 30% of export production, corresponding to N_2 fixation rates of 0 ± 336 μmol N m^{-2} d^{-1} (Table I). The detection of N_2 fixation during the 2017 and not 2018 cycles is consistent with the higher, albeit still very low, abundance of *Trichodesmium* spp. in 2017 vs. 2018 (Fig. 5; Selph *et al.*, 2021). These geochemically derived N_2 fixation rates are also consistent with the range of previously reported $^{15}N_2$ uptake rates from the northern GoM (Redalje *et al.*, 2019) and references therein. In particular, (Weber *et al.*, 2016) reported low rates of 0.07–0.37 nmol N L^{-1} d^{-1} in July 2013 near the northern GoM shelf break, while (Holl *et al.*, 2007) reported July 2000 rates of 85 ± 18 μmol N m^{-2} d^{-1} from sites near to this study area. This range in previously reported $^{15}N_2$ uptake rates largely brackets the geochemical estimates of N_2 fixation rates from this study (Table I). The N_2 fixation rates estimated from these $\delta^{15}N$ budgets are relatively low compared with those found throughout the global ocean (Luo *et al.*, 2012), and are consistent with previous work that found a minor role for N_2 fixation supporting export production in the nearby Sargasso Sea (Altabet, 1988, Fawcett *et al.*, 2011, Knapp *et al.*, 2005).

We note that low rates of N_2 fixation (<50 μmol N m^{-2} d^{-1}) by all diazotrophs may have occurred in the study region and not been detected by the $\delta^{15}N$ budget (Knapp *et al.*, 2005). However, prior work in the Arabian Sea comparing *Trichodesmium* spp. trichome abundance and PN_{sink} $\delta^{15}N$ only observed a depression in the $\delta^{15}N$ of PN_{sink} when >2000 trichomes L^{-1} were observed (Capone *et al.*, 1998). To explore the quantitative potential for N_2 fixation by *Trichodesmium* spp. at the trichome abundances observed in this study to influence the $\delta^{15}N$ of PN_{susp} and/or the $\delta^{15}N$ of DON, we consider the following. If there were 10 *Trichodesmium* spp. trichomes L^{-1} in all of our study locations and times (Fig. 5) (Selph *et al.*, 2021) fixing at a rate of 1.0 pmol N $trichome^{-1}$ hr^{-1} (Capone *et al.*, 1998), and N_2 fixation occurred over a 12-hour photoperiod, that would correspond to 120 pM N fixed d^{-1}. We could further make the (unrealistic) assumption that all of that newly fixed N accumulated as DON, none went into *Trichodesmium* spp. biomass, none went into higher trophic levels, no *Trichodesmium* spp. sank out (Hewson *et al.*, 2007, Marumo & Asaoka, 1974), and none of the DON was advected away due to circulation. Making the same assumptions to maximize newly fixed N accumulation in the DON pool, and sustaining that rate of N_2 fixation over 100 days, this would only correspond to an accumulation of 12 nM DON. This quantity of newly fixed N would not be detectable in terms of concentration or isotopic composition in the DON or PN_{susp} pools (Knapp *et al.*, 2008, Knapp *et al.*, 2005, Knapp *et al.*, 2011). In contrast to the mass and isotopic inertia of the PN_{susp} and especially the DON pools, the short-time period over which the PN_{sink} flux integrates over means the PN_{sink} flux is the most responsive to small changes in the relative source of new N fueling export, and thus the best target for detecting N_2 fixation inputs (Altabet, 1988, Karl *et al.*, 1997). Given that Thorpe-scale analyses indicate that vertical NO_3^- transport at the time of sampling was low, N fueling the PN_{sink} flux may have originated from upwelling of NO_3^- near the shelf break (Sharples *et al.*, 2009, Sharples *et al.*, 2007) and lateral advection of resulting organic N (Kelly *et al.*, 2021). Finally, we note that while we have assumed that any low-$\delta^{15}N$ inputs to the system are from N_2 fixation, the rate of N_2 fixation estimated by the $\delta^{15}N$ budget for Cycle 2, 90 μmol N m^{-2} d^{-1} (Table I) is comparable to rates of atmospheric $NO_3^- + NO_2^-$ deposition in the region, 20–30 μmol N m^{-2} d^{-1} (Hastings *et al.*, 2003, Katz *et al.*, 2009, Prospero *et al.*, 1996), which has a similarly low $\delta^{15}N$ (Dillon & Chanton, 2005, Hastings *et al.*, 2003, Knapp *et al.*, 2010). Given the low diazotroph abundance observed on these cruises (Selph *et al.*, 2021), atmospheric deposition of low-$\delta^{15}N$ N may contribute to the low-$\delta^{15}N$ PN_{sink} flux observed in Cycle 2.

Mixed layer vs. subeuphotic zone PN_{sink} $\delta^{15}N$: the $\delta^{15}N$ associated with regenerated production

To the best of our knowledge, the PN_{sink} flux and its $\delta^{15}N$ have not been reported from sediment traps deployed *within* the euphotic zone before. The results from this study show that the PN_{sink} flux leaving the upper euphotic zone typically exceeds the PN_{sink} flux leaving the base of the euphotic zone. On the NF1802 cruise, the PN_{sink} flux in the subeuphotic zone trap was 81% (C4) and 82% (C5) of the PN_{sink} flux captured in the 60-m trap. On the NF1704 cruise, this ratio varied from 30 to 112% (although the C3 measurement of 112% was not significantly different from the PN_{sink} flux measured in the 60-m trap) (Table I). Taken together, these results suggest that more particles were consumed in the vicinity of the deep chlorophyll maximum than were produced at that depth, with the net consumption of those particles contributing to regenerated production (Stukel *et al.*, 2021). Importantly, the $\delta^{15}N$ of the PN_{sink} flux in the 60 m traps was 0.4–2.0‰ lower than that in the deeper traps in all cycles (Fig. 2) (Table I). The $\delta^{15}N$ of the PN_{sink} flux in the 50 m traps ranged from 1.6 ± 0.3‰ to 3.8 ± 0.2‰ (Table I). Interestingly, although perhaps not surprising given the small sample size, the $\delta^{15}N$ increase between the 60 m and mid-depth traps does not appear related to the ratio of the PN_{sink} flux captured in the mid-depth vs. euphotic zone traps, which would be expected if flux attenuation between the traps was significant and associated with an isotope effect for N degradation. Regardless, the difference in $\delta^{15}N$ of the PN_{sink} flux between the euphotic and subeuphotic zone is consistent with regenerated production supported by low-$\delta^{15}N$ N. This is also consistent with high rates of NH_4^+ regeneration that have been found in the northern GoM to be the primary source of N fueling primary productivity (Bode & Dortch, 1996, Wawrik *et al.*, 2004). Regenerated NH_4^+ is expected to be relatively low in $\delta^{15}N$ whether it originates from zooplankton excretion (Checkley & Miller, 1989) (Deniro & Epstein, 1981, Minagawa & Wada, 1984, Wada *et al.*, 1987), or from the degradation of DON (Knapp *et al.*, 2018a, Knapp *et al.*, 2011, Zhang *et al.*, 2020) or PN_{susp} (Hannides *et al.*, 2013). Moreover, multiple lines of evidence indicate that low-$\delta^{15}N$ forms of N accumulate in the pools associated with regenerated production. Near Bermuda, (Altabet, 1988) showed that the $\delta^{15}N$ of PN_{susp} was ~3‰ lower than that of PN_{sink}, whereas the $\delta^{15}N$ of PN_{sink} was roughly equivalent to that of subsurface NO_3^-. Later, (Fawcett *et al.*, 2011) found that low-$\delta^{15}N$ N sources supported the organisms carrying out regenerated production near Bermuda. Additionally, they found that the $\delta^{15}N$ of eukaryotic phytoplankton near Bermuda was elevated compared to cyanobacteria and heterotrophic microbes. The $\delta^{15}N$ of the eukaryotes was similar to that of subsurface NO_3^- and the PN_{sink} flux, whereas the $\delta^{15}N$ of cyanobacteria was similar to the $\delta^{15}N$ of the bulk PN_{susp} pool and 1–5‰ lower than the $\delta^{15}N$ of subsurface NO_3^- (Fawcett *et al.*, 2011). Together, this evidence indicates that the $\delta^{15}N$ of regenerated N retained in the euphotic zone should be 1–6‰ lower than the $\delta^{15}N$ of the dominant source of N to surface waters, whereas the $\delta^{15}N$ of fluxes of N to and from should be roughly equivalent. Thus, the magnitude of the $\delta^{15}N$ increase between the shallow and mid-depth traps observed in the GoM is broadly consistent with the mechanisms outlined above that would retain low-$\delta^{15}N$ material in the euphotic zone to support regenerated production and permit elevated $\delta^{15}N$ to leave via the PN_{sink} flux.

Interestingly, the $\delta^{15}N$ of the PN_{sink} flux captured in the 60 m traps, 1.6–3.8‰ (Table I), is relatively high compared to the $\delta^{15}N$ of PN_{susp}, 1.2–2.5‰ (Fig. 5), suggesting that the 60 m PN_{sink} flux is supported by allochthonous sources of N, such as subsurface NO_3^-, and/or is produced by organisms feeding relatively high in the food chain. Additionally, the $\delta^{15}N$ of PN_{susp} is elevated compared to that collected near Bermuda, −1 to 0‰ (Altabet, 1988, Fawcett *et al.*, 2011). The differences in the $\delta^{15}N$ of PN_{susp} from the GoM and near Bermuda qualitatively indicate that NO_3^- is an even more important source of new N to surface waters and/or that the ratio of new to regenerated production is higher in the GoM than near Bermuda. Thus, the isotopic evidence overwhelmingly indicates that subsurface NO_3^-, and not N_2 fixation, supports export production in these GoM samples. However, we acknowledge the possibility that PN_{sink} with a $\delta^{15}N$ between 2.8 and 4.9‰ could also result from a linear combination of lateral sources of N with a relatively high $\delta^{15}N$, potentially including Mississippi River and/or other coastal sources, with sources of low-$\delta^{15}N$ N, including N_2 fixation, atmospheric deposition and/or the consumption of DON with an isotope effect (Knapp *et al.*, 2018a, Zhang *et al.*, 2020). None of our other measurements, however, show any clear evidence of substantial riverine or diazotrophic influence (Selph *et al.*, 2021). We also note that our results reflect a relatively short-sampling period, and so does not preclude N_2 fixation supporting a higher fraction of export at other times.

CONCLUSIONS

Here we use a geochemical tool, a $\delta^{15}N$ budget, to evaluate the sources of new N fueling export production in the oceanic GoM. Measurements of water-column $NO_3^- + NO_2^-$ $\delta^{15}N$ were compared with the $\delta^{15}N$ of

PN_{sink} captured in floating sediment traps deployed below the euphotic zone. The results of the $\delta^{15}N$ budgets indicate that subsurface $NO_3^- + NO_2^-$, not N_2 fixation, is the dominant source of new N supporting export production in samples collected in the deep waters of the GoM in May of 2017 and 2018. Geochemically estimated N_2 fixation rates, when N_2 fixation was detected at all, were low and consistent with prior $^{15}N_2$ uptake rates reported from the northern GoM (Holl *et al.*, 2007). We also report the first measurements of DON $\delta^{15}N$ from the GoM, which are similar to prior observations from the Sargasso Sea (Knapp *et al.*, 2005, Knapp *et al.*, 2011). Finally, the difference in the $\delta^{15}N$ of PN_{sink} collected in the shallow vs. mid-depth sediment traps is consistent with regenerated production having a low $\delta^{15}N$ compared to the $\delta^{15}N$ of the PN_{sink} flux captured below the euphotic zone.

DATA ARCHIVING

Data presented here have been submitted to the National Oceanic and Atmospheric Administration's (NOAA) National Centers for Environmental Information (NCEI) data repository, and are also archived at the BCO-DMO (Biological and Chemical Oceanography Data Management Office) site: https://www.bco-dmo.org/project/819488.

ACKNOWLEDGEMENTS

We gratefully acknowledge the crew and science parties on the *NOAA Ship* Nancy Foster cruises who collected these samples as well as colleagues in the BLOOFINZ-GoM project for discussions.

FUNDING

This work was supported by a National Oceanic and Atmospheric Administration's RESTORE Program Grant (Project Title: Effects of N sources and plankton food-web dynamics on habitat quality for the larvae of Atlantic bluefin tuna in the Gulf of Mexico) under federal funding opportunity NOAA-NOS-NCCOS-2017-2004875. https://restoreactscienceprogram.noaa.gov/funded-projects/bluefin-tuna-larvae. This study acknowledges BLOOFINZ Program support from National Oceanic and Atmospheric Administration awards NA15OAR4320071 (to M.R.L.), NA16NMF4320058 (to K.E.S.), NA15OAR4320064 (to A.N.K. and M.R.S.) and U.S. National Science Foundation award OCE-1851558 (M.R.L.) and OCE-1851347 (A.N.K., M.R.S.).

REFERENCES

Altabet, M. A. (1988) Variations in nitrogen isotopic composition between sinking and suspended particles - implications for nitrogen cycling and particle transformation in the open ocean. *Deep Sea Res. Part A Oceanograph. Res. Paper.*, **35**, 535–554.

Altabet, M. A., Deuser, W. G., Honjo, S. and Stienen, C. (1991) Seasonal and depth-related changes in the source of sinking particles in the North-Atlantic. *Nature*, **354**, 136–139.

Amon, R. M. W., Ochoa, J., Candela, J., Sheinbaum, J., Herguera, J. C., Herzka, S. Z., Perez-Brunius, P., Hernandez-Ayon, J. M. *et al.* (2020, 2020) Novel insights into deep ventilation of the Gulf of Mexico and its linkage to the Labrador Sea. *Ocean Sciences Meeting*.

Berman-Frank, I., Cullen, J. T., Shaked, Y., Sherrell, R. M. and Falkowski, P. G. (2001) Iron availability, cellular iron quotas, and nitrogen fixation in Trichodesmium. *Limnol. Oceanogr.*, **46**, 1249–1260.

Bidigare, R. (1983) Nitrogen excretion by marine zooplankton. In Carpenter, E. J. and Capone, D. G. (eds.), *Nitrogen in the Marine Environment*, 1st edn, Academic Press, New York, pp. 385–409.

Bode, A. and Dortch, Q. (1996) Uptake and regeneration of inorganic nitrogen in coastal waters influenced by the Mississippi River spatial and seasonal variations. *J. Plankton Res.*, **18**, 2251–2268.

Bonnet, S., Berthelot, H., Turk-Kubo, K., Fawcett, S., Rahav, E., L'helguen, S. and Berman-Frank, I. (2016) Dynamics of N2 fixation and fate of diazotroph-derived nitrogen during the VAHINE mesocosm experiment. *Biogeosciences*, **13**, 2653–2673.

Bourbonnais, A., Lehmann, M. F., Waniek, J. J. and Schulz-Bull, D. E. (2009) Nitrate isotope anomalies reflect N-2 fixation in the Azores front region (subtropical NE Atlantic). *J. Geophys. Res. Oceans*, **114**, C03003. doi: 10.1029/2007JC004617.

Braman, R. S. and Hendrix, S. A. (1989) Nanogram nitrite and nitrate determination in environmental and biological-materials by vanadium(III) reduction with Chemi luminescence detection. *Anal. Chem.*, **61**, 2715–2718.

Breitbarth, E., Oschlies, A. and Laroche, J. (2007) Physiological constraints on the global distribution of Trichodesmium - effect of temperature on diazotrophy. *Biogeosciences*, **4**, 53–61.

Bronk, D. A. and Ward, B. B. (1999) Gross and net nitrogen uptake and DON release in the euphotic zone of Monterey Bay, California. *Limnol. Oceanogr.*, **44**, 573–585.

Bronk, D. A. and Ward, B. B. (2000) Magnitude of dissolved organic nitrogen release relative to gross nitrogen uptake in marine systems. *Limnol. Oceanogr.*, **45**, 1879–1883.

Bronk, D. A. and Ward, B. B. (2005) Inorganic and organic nitrogen cycling in the Southern California Bight. *Deep Sea Res. Part I-Oceanograph. Research Paper.*, **52**, 2285–2300.

Caffin, M., Moutin, T., Foster, R.A., Bouruet-Aubertot, P., Doglioli, A.M., Berthelot, H., Guieu, C., Grosso, O., Helias-Nunige, S., Leblond, N., Gimenez, A., Petrenko, A.A., deVerneil, A., and S. Bonnet (2018) N2 fixation as dominant new N source in the western tropical South Pacific Ocean (OUTPACE cruise). *Biogeosci.*, **15**, 2565–2585.

Capone, D. G., Burns, J. A., Montoya, J. P., Subramaniam, A., Mahaffey, C., Gunderson, T., Michaels, A. F. and Carpenter, E. J. (2005) Nitrogen fixation by Trichodesmium spp.: an important source of new nitrogen to the tropical and subtropical North Atlantic Ocean. *Global Biogeochem. Cycles*, **19**, GB2024. doi: 10.1029/2004GB002331.

Capone, D. G., Subramaniam, A., Montoya, J. P., Voss, M., Humborg, C., Johansen, A. M., Siefert, R. L. and Carpenter, E. J. (1998) An extensive bloom of the N(2)-fixing cyanobacterium Trichodesmium erythraeum in the central Arabian Sea. *Mar. Ecol. Prog. Ser.*, **172**, 281–292.

Capone, D. G., Zehr, J. P., Paerl, H. W., Bergman, B. and Carpenter, E. J. (1997) Trichodesmium, a globally significant marine cyanobacterium. *Science*, **276**, 1221–1229.

Capotondi, A., Alexander, M. A., Bond, N. A., Curchitser, E. N. and Scott, J. D. (2012) Enhanced upper ocean stratification with climate change in the CMIP3 models. *J. Geophys. Res. Oceans*, **117**, C04031. doi: 10.1029/2011JC007409.

Carpenter, E. J., Harvey, H. R., Fry, B. and Capone, D. G. (1997) Biogeochemical tracers of the marine cyanobacterium Trichodesmium. *Deep Sea Res. Part I Oceanograph. Res. Paper.*, **44**, 27–38.

Carpenter, E. J., Subramaniam, A. and Capone, D. G. (2004) Biomass and primary productivity of the cyanobacterium Trichodesmium spp. in the tropical N Atlantic Ocean. *Deep Sea Res. Part I-Oceanograph. Res. Paper.*, **51**, 173–203.

Casciotti, K. L., Sigman, D. M., Hastings, M. G., Bohlke, J. K. and Hilkert, A. (2002) Measurement of the oxygen isotopic composition of nitrate in seawater and freshwater using the denitrifier method. *Anal. Chem.*, **74**, 4905–4912.

Casciotti, K. L., Trull, T. W., Glover, D. M. and Davies, D. (2008) Constraints on nitrogen cycling at the subtropical North Pacific Station ALOHA from isotopic measurements of nitrate and particulate nitrogen. *Deep Sea Res. Part II Topical Stud. Oceanograph.*, **55**, 1661–1672.

Checkley, D. M. and Entzeroth, L. C. (1985) Elemental and isotopic fractionation of carbon and nitrogen by marine, planktonic copepods and implications to the marine nitrogen-cycle. *J. Plankton Res.*, **7**, 553–568.

Checkley, D. M. and Miller, C. A. (1989) Nitrogen isotope fractionation by oceanic zooplankton. *Deep Sea Res. Part a Oceanograph. Res. Paper.*, **36**, 1449–1456.

Christian, J. R., Lewis, M. R. and Karl, D. M. (1997) Vertical fluxes of carbon, nitrogen, and phosphorus in the North Pacific subtropical gyre near Hawaii. *J. Geophys. Res. Oceans*, **102**, 15667–15677.

Cutter, G. A., Andersson, P., Codispoti, L., Croot, P., Francois, R., Lohan, M., Obata, H. and Van Der Loeff, M. R. (2010) *Sampling and Sample-handling Protocols for GEOTRACES Cruises*, GEOTRACES, Norfolk. p. 145.

DeNiro, M. J. and Epstein, S. (1981) Influence of diet on the distribution of nitrogen isotopes in animals. *Geochim. Cosmochim. Acta*, **45**, 341–351.

Dillon, K. S. and Chanton, J. P. (2005) Nutrient transformations between rainfall and stormwater runoff in an urbanized coastal environment: Sarasota Bay, Florida. *Limnol. Oceanogr.*, **50**, 62–69.

Dore, J.E., Brum, J.R., Tupas, L.M., and Karl, D.M. (2002) Seasonal and interannual variability in sources of nitrogen supporting export in the oligotrophic subtropical North Pacific Ocean. *Limnol. Oceanogr.*, **47**(6), 1595–1607.

Dugdale, R. C. and Goering, J. J. (1967) Uptake of new and regenerated forms of nitrogen in primary productivity. *Limnol. Oceanogr.*, **12**, 196.

Emerson, S. (2014) Annual net community production and the biological carbon flux in the ocean. *Global Biogeochem. Cycles*, **28**, 2013GB004680.

Eppley, R. W. and Peterson, B. J. (1979) Particulate organic-matter flux and planktonic new production in the deep ocean. *Nature*, **282**, 677–680.

Falkowski, P. G., Ziemann, D., Kolber, Z. and Bienfang, P. K. (1991) Role of eddy pumping in enhancing primary production in the ocean. *Nature*, **352**, 55–58.

Fawcett, S. E., Lomas, M., Casey, J. R., Ward, B. B. and Sigman, D. M. (2011) Assimilation of upwelled nitrate by small eukaryotes in the Sargasso Sea. *Nat. Geosci.*, **4**, 717–722.

Fujiki, L. A., Santiago-Mandujano, F., Lethaby, P., Lukas, R. and Karl, D. (2011, 2008) *Hawaii Ocean Time-series Data Report 20*, University of Hawaii, Honolulu. p. 395.

Gerard, T., Lamkin, J., Kelly, T., Knapp, A., Laiz-Carrion, R., Malca, E., Selph, K., Shiroza, A. *et al.* (In Review) Bluefin larvae in oligotrophic ocean foodwebs, investigations of nutrients to zooplankton: overview of the BLOOFINZ-Gulf of Mexico program. *J. Plankton Res.*.

Granger, J., Sigman, D. M., Needoba, J. A. and Harrison, P. J. (2004) Coupled nitrogen and oxygen isotope fractionation of nitrate during assimilation by cultures of marine phytoplankton. *Limnol. Oceanogr.*, **49**, 1763–1773.

Hannides, C. C. S., Popp, B. N., Choy, C. A. and Drazen, J. C. (2013) Midwater zooplankton and suspended particle dynamics in the North Pacific subtropical gyre: a stable isotope perspective. *Limnol. Oceanogr.*, **58**, 1931–1946.

Hannides, C. C. S., Popp, B. N., Landry, M. R. and Graham, B. S. (2009) Quantification of zooplankton trophic position in the North Pacific subtropical gyre using stable nitrogen isotopes. *Limnol. Oceanogr.*, **54**, 50–61.

Hastings, M. G., Sigman, D. M. and Lipschultz, F. (2003) Isotopic evidence for source changes of nitrate in rain at Bermuda. *J. Geophys. Res. Atmosphere*, **108**(D24), 4790. doi: 10.1029/2003JD003789.

Hernandez-Guerra, A. and Joyce, T. M. (2000) Water masses and circulation in the surface layers of the Caribbean at 66 W. *Geophys. Res. Lett.*, **27**, 3497–3500.

Hewson, I., Moisander, P. H., Achilles, K. M., Carlson, C. A., Jenkins, B. D., Mondragon, E. A., Morrison, A. E. and Zehr, J. P. (2007) Characteristics of diazotrophs in surface to abyssopelagic waters of the Sargasso Sea. *Aquat. Microb. Ecol.*, **46**, 15–30.

Hoering, T. C. and Ford, H. T. (1960) The isotope effect in the fixation of nitrogen by Azotobacter. *J. Am. Chem. Soc.*, **82**, 376–378.

Hofmann, E. E. and Worley, S. J. (1986) An investigation of the circulation of the Gulf of Mexico. *J. Geophys. Res. Oceans*, **91**, 14221–14236.

Holl, C. M., Villareal, T. A., Payne, C. D., Clayton, T. D., Hart, C. and Montoya, J. P. (2007) Trichodesmium in the western Gulf of Mexico: 15N2-fixation and natural abundance stable isotope evidence. *Limnol. Oceanogr.*, **52**, 2249–2259.

Holmes, R. M., Aminot, A., Kerouel, R., Hooker, B. A. and Peterson, B. J. (1999) A simple and precise method for measuring ammonium in marine and freshwater ecosystems. *Can. J. Fish. Aquat. Sci.*, **56**, 1801–1808.

Howe, S., Miranda, C., Hayes, C., Letscher, R. and Knapp, A. N. (2020) The dual isotopic composition of nitrate in the Gulf of Mexico and Florida Straits. *J. Geophys. Res. Oceans*, **125**, e2020JC016047.

Hung, C.C., Guo, L.D., Roberts, K.A., and P.H. Santschi (2004) Upper ocean carbon flux determined by the (234)Th approach and sediment traps using size-fractionated POC and (234) Th data from the Gulf of Mexico. *Geochem. J.*, **38**(6), 601–611.

Hung, C.-C., Xu, C., Santschi, P.H., Zhang, S.-J., Schwehr, K.A., Quigg, A., Guo, L., Gong, G.-C., Pinckney, J.L., Long, R.A., and Wei, C.-L. (2010) Comparative evaluation of sediment trap and 234Th-derived POC fluxes from the upper oligotrophic waters of the Gulf of Mexico and the subtropical northwestern Pacific Ocean. *Mar. Chem.*, **121**(1), 132–144.

Ikeda, T. (1985) Metabolic rates of epipelagic marine zooplankton as a function of body mass and temperature. *Mar. Biol.*, **85**(1), 1–11.

Karl, D., Letelier, R., Tupas, L., Dore, J., Christian, J. and Hebel, D. (1997) The role of nitrogen fixation in biogeochemical cycling in the subtropical North Pacific Ocean. *Nature*, **388**, 533–538.

Katz, B. G., Sepulveda, A. A. and Verdi, R. J. (2009) Estimating nitrogen loading to ground water and assessing vulnerability to nitrate contamination in a large Karstic Springs basin, Florida. *J. Am. Water Resour. Assoc.*, **45**, 607–627.

Kelly, T. B., Knapp, A. N., Landry, M. R., Selph, K. E., Shropshire, T. A., Thomas, R. and Stukel, M. R. (2021) Lateral advection supports nitrogen export in the oligotrophic open-ocean Gulf of Mexico. *Nat. Commun.*, **12**, 1–7.

Knapp, A. N., Casciotti, K. L., Berelson, W. M., Prokopenko, M. G. and Capone, D. G. (2016a) Low rates of nitrogen fixation in eastern tropical South Pacific surface waters. *Proc. Natl. Acad. Sci. U. S. A.*, **113**, 4398–4403.

Knapp, A. N., Casciotti, K. L. and Prokopenko, M. G. (2018a) Dissolved organic nitrogen production and consumption in eastern tropical South Pacific surface waters. *Global Biogeochem. Cycles*, **32**, 769–783.

Knapp, A. N., Difiore, P. J., Deutsch, C., Sigman, D. M. and Lipschultz, F. (2008) Nitrate isotopic composition between Bermuda and Puerto Rico: implications for N(2) fixation in the Atlantic Ocean. *Global Biogeochem. Cycles*, **22**, GB3014. doi: 10.1029/2007GB003107.

Knapp, A. N., Fawcett, S. E., Martínez-Garcia, A., Leblond, N., Moutin, T. and Bonnet, S. (2016b) Nitrogen isotopic evidence for a shift from nitrate- to diazotroph-fueled export production in the VAHINE mesocosm experiments. *Biogeosciences*, **13**, 4645–4657.

Knapp, A. N., Hastings, M. G., Sigman, D. M., Lipschultz, F. and Galloway, J. N. (2010) The flux and isotopic composition of reduced and total nitrogen in Bermuda rain. *Mar. Chem.*, **120**, 83–89.

Knapp, A. N., Mccabe, K. M., Grosso, O., Leblond, N., Moutin, T. and Bonnet, S. (2018b) Distribution and rates of nitrogen fixation in the western tropical South Pacific Ocean constrained by nitrogen isotope budgets. *Biogeosciences*, **15**, 2619–2628.

Knapp, A. N., Sigman, D. M. and Lipschultz, F. (2005) N isotopic composition of dissolved organic nitrogen and nitrate at the Bermuda Atlantic time-series study site. *Global Biogeochem. Cycles*, **19**, GB1018. doi: 10.1029/2004GB002320.

Knapp, A. N., Sigman, D. M., Lipschultz, F., Kustka, A. B. and Capone, D. G. (2011) Interbasin isotopic correspondence between upper-ocean bulk DON and subsurface nitrate and its implications for marine nitrogen cycling. *Global Biogeochem. Cycles*, **25**, GB4004. doi: 10.1029/2010GB003878.

Koroleff, F. (1983) Determination of nutrients. In Grasshoff, K., Ehrherd, M. and Kremling, K. (eds.), *Methods of Seawater Analysis*, 2nd edn, Springer Verlag Chemie, Weinheim. pp. 125–135.

Kustka, A. B., Sanudo-Wilhelmy, S. A., Carpenter, E. J., Capone, D., Burns, J. and Sunda, W. G. (2003) Iron requirements for dinitrogen- and ammonium-supported growth in cultures of Trichodesmium (IMS 101): comparison with nitrogen fixation rates and iron: carbon ratios of field populations. *Limnol. Oceanogr.*, **48**, 1869–1884.

Landry, M.R., Hussain, A.-M., Selph, K.E., Christensen, S., and S. Nunnery (2001) Seasonal patterns of mesozooplankton abundance and biomass at Station ALOHA. *Deep-Sea Res. II*, **48**(8), 2037–2061.

Landry, M. R. and Swalethorp, R. (2021) Mesozooplankton biomass, grazing and trophic structure in the bluefin tuna spawning area of the oceanic Gulf of Mexico. *J. Plankton Res.*. 10.1093/plankt/fbab008.

Leichter, J. J., Paytan, A., Wankel, S. and Hanson, K. (2007) Nitrogen and oxygen isotopic signatures of subsurface nitrate seaward of the Florida keys reef tract. *Limnol. Oceanogr.*, **52**, 1258–1267.

Luo, Y.-W., Shi, D., Kranz, S. A., Hopkinson, B. M., Hong, H., Shen, R. and Zhang, F. (2019) Reduced nitrogenase efficiency dominates response of the globally important nitrogen fixer Trichodesmium to ocean acidification. *Nat. Commun.*, **10**, 1521.

Luo, Y. W., Doney, S. C., Anderson, L. A., Benavides, M., Berman-Frank, I., Bode, A., Bonnet, S., Boström, K. H. *et al.* (2012) Database of diazotrophs in global ocean: abundance, biomass and nitrogen fixation rates. *Earth Syst. Sci. Data*, **4**, 47–73.

Mahaffey, C., Michaels, A. F. and Capone, D. G. (2005) The conundrum of marine N(2) fixation. *Am. J. Sci.*, **305**, 546–595.

Mahowald, N. M., Engelstaedter, S., Luo, C., Sealy, A., Artaxo, P., Benitez-Nelson, C., Bonnet, S., Chen, Y. *et al.* (2009) Atmospheric iron deposition: global distribution, variability, and human perturbations. *Ann. Rev. Mar. Sci.*, **1**, 245–278.

Maiti, K., Bosu, S., D'Sa, E.J., Adhikari, P.L., Sutor, M., and K. Longnecker (2016) Export fluxes in northern Gulf of Mexico - Comparative evaluation of direct, indirect and satellite-based estimates. *Mar. Chem.*, **184**, 60–77.

Marconi, D., Sigman, D. M., Casciotti, K. L., Campbell, E. C., Weigand, M. A., Fawcett, S. E., Knapp, A. N., Rafter, P. A. *et al.* (2017) Tropical dominance of N2 fixation in the North Atlantic Ocean. *Global Biogeochem. Cycles*, **31**, 1608–1623.

Marconi, D., Weigand, M. A., Rafter, P. A., McIlvin, M. R., Forbes, M., Casciotti, K. L. and Sigman, D. M. (2015) Nitrate isotope distributions on the US GEOTRACES North Atlantic cross-basin section: signals of polar nitrate sources and low latitude nitrogen cycling. *Mar. Chem.*, **177**, 143–156.

Marconi, D., Weigand, M. A. and Sigman, D. M. (2019) Nitrate isotopic gradients in the North Atlantic Ocean and the nitrogen isotopic composition of sinking organic matter. *Deep Sea Res. I Oceanogr. Res. Pap.*, **145**, 109–124.

Marumo, R. and Asaoka, O. (1974) Distribution of pelagic blue-green algae in the North Pacific Ocean. *J. Oceanograph. Soc. Japan*, **30**, 77–85.

McClelland, J. W., Holl, C. M. and Montoya, J. P. (2003) Relating low delta N-15 values of zooplankton to N-2-fixation in the tropical North Atlantic: insights provided by stable isotope ratios of amino acids. *Deep Sea Res. Part I Oceanograph. Res. Paper.*, **50**, 849–861.

McIlvin, M. R. and Casciotti, K. L. (2011) Technical updates to the bacterial method for nitrate isotopic analyses. *Anal. Chem.*, **83**, 1850–1856.

Minagawa, M. and Wada, E. (1984) Stepwise enrichment of N-15 along food-chains - further evidence and the relation between Delta-N-15 and animal age. *Geochim. Cosmochim. Acta*, **48**, 1135–1140.

Minagawa, M. and Wada, E. (1986) Nitrogen isotope ratios of red tide organisms in the East-China-Sea - a characterization of biological nitrogen-fixation. *Mar. Chem.*, **19**, 245–259.

Monterey, G. and Levitus, S. (1997) Seasonal variability of mixed layer depth for the world ocean. In *D. O. C. NOAA, USA (ed)*, Vol. **14**, NOAA, Silver Spring, MD, p. 100.

Montoya, J. P., Carpenter, E. J. and Capone, D. G. (2002) Nitrogen fixation and nitrogen isotope abundances in zooplankton of the oligotrophic North Atlantic. *Limnol. Oceanogr.*, **47**, 1617–1628.

Morey, S. L., Martin, P. J., O'Brien, J. J., Wallcraft, A. A. and Zavala-Hidalgo, J. (2003) Export pathways for river discharged fresh water in the northern Gulf of Mexico. *J. Geophys. Res. Oceans*, **108**(C10), 3303. doi: 10.1029/2002JC001674.

Morrison, J. M., Merrell, W. J. Jr., Key, R. M. and Key, T. C. (1983) Property distributions and deep chemical measurements within the western Gulf of Mexico. *J. Geophys. Res. Oceans*, **88**, 2601–2608.

Mulholland, M. R., Bernhardt, P. W., Heil, C. A., Bronk, D. A. and O'Neil, J. M. (2006) Nitrogen fixation and release of fixed nitrogen by Trichodesmium spp. in the Gulf of Mexico. *Limnol. Oceanogr.*, **51**, 1762–1776.

Mulholland, M. R., Bernhardt, P. W., Ozmon, I., Procise, L. A., Garrett, B. M., O'Neil, J. M., Heil, C. A. and Bronk, D. A. (2014) Contribution of diazotrophy to nitrogen inputs supporting Karenia brevis blooms in the Gulf of Mexico. *Harmful Algae*, **38**, 20–29.

Owens, N.J.P., and A.P. Rees (1989) Determination of N-15 at Sub-microgram Levels of Nitrogen Using Automated Continuous-Flow Isotope Ratio Mass-Spectrometry. *Analyst*, **114**(12), 1655–1657.

Press, W. H., Teukolsky, S. A., Vetterling, W. T. and Flannery, B. P. (1992) *Numerical Recipes in C: The Art of Scientific Computing*, 2nd edn, Cambridge University Press, Cambridge.

Prospero, J. M. (1996) Saharan dust transport over the North Atlantic Ocean and Mediterranean: an overview. *Impact Desert Dust across the Mediterranean*, **11**, 133–151.

Prospero, J. M., Barrett, K., Church, T., Dentener, F., Duce, R. A., Galloway, J. N., Levy, H., Moody, J. *et al.* (1996) Atmospheric deposition of nutrients to the North Atlantic Basin. *Biogeochemistry*, **35**, 27–73.

Redalje, D. G., Ammerman, J., Herrerra, J., Knapp, A., Krause, J., Valdes, D. and Hayward, A. (2019) Nutrients in the Gulf of Mexico: Distributions, Cycles, Sources, Sinks and Processes. In: T. S. Bianchi (ed) *Gulf of Mexico Origin, Waters, and Biota*. Texas A&M University Press, College Station. pp. 294.

Sanial, V., Moore, W. S. and Shiller, A. M. (2021) Does a bottom-up mechanism promote hypoxia in the Mississippi Bight? *Mar. Chem.*, **235**, 104007.

Selph, K. E., Swalethorp, R., Stukel, M. R., Kelly, T. B., Knapp, A. N., Fleming, K., Hernandez, T. and Landry, M. R. (2021) Phytoplankton community composition and biomass in the oligotrophic Gulf of Mexico. *J. Plankton Res*. 10.1093/plankt/fbab006.

Sharples, J., Moore, C. M., Hickman, A. E., Holligan, P. M., Tweddle, J. F., Palmer, M. R. and Simpson, J. H. (2009) Internal tidal mixing as a control on continental margin ecosystems. *Geophys. Res. Lett.*, **36**, L23603. doi: 10.1029/2009GL040683.

Sharples, J., Tweddle, J. F., Mattias Green, J. A., Palmer, M. R., Kim, Y.-N., Hickman, A. E., Holligan, P. M., Moore, C. M. *et al.* (2007) Spring-neap modulation of internal tide mixing and vertical nitrate fluxes at a shelf edge in summer. *Limnol. Oceanogr.*, **52**, 1735–1747.

Shi, D., Kranz, S. A., Kim, J.-M. and Morel, F. M. M. (2012) Ocean acidification slows nitrogen fixation and growth in the dominant diazotroph Trichodesmium under low-iron conditions. *Proc. Natl. Acad. Sci. U.S.A.*, **109**, E3094–E3100.

Shiozaki, T., Bombar, D., Riemann, L., Sato, M., Hashihama, F., Kodama, T., Tanita, I., Takeda, S. *et al.* (2018) Linkage between dinitrogen fixation and primary production in the oligotrophic South Pacific Ocean. *Global Biogeochem. Cycles*, **32**, 1028–1044.

Sigman, D. M., Casciotti, K. L., Andreani, M., Barford, C., Galanter, M. and Bohlke, J. K. (2001) A bacterial method for the nitrogen isotopic analysis of nitrate in seawater and freshwater. *Anal. Chem.*, **73**, 4145–4153.

Sohm, J. A., Webb, E. A. and Capone, D. G. (2011) Emerging patterns of marine nitrogen fixation. *Nat. Rev. Microbiol.*, **9**, 499–508.

Stal, L. J. (2009) Is the distribution of nitrogen-fixing cyanobacteria in the oceans related to temperature? *Environ. Microbiol.*, **11**, 1632–1645.

Stenegren, M., Caputo, A., Berg, C., Bonnet, S. and Foster, R. A. (2018) Distribution and drivers of symbiotic and free-living diazotrophic cyanobacteria in the western tropical South Pacific. *Biogeosciences*, **15**, 1559–1578.

Stukel, M. R., Décima, M., Landry, M. R. and Selph, K. E. (2018) Nitrogen and isotope flows through the Costa Rica dome upwelling ecosystem: the crucial Mesozooplankton role in export flux. *Global Biogeochem. Cycles*, **32**, 1815–1832.

Stukel, M. R., Kelly, T. B., Landry, M. R., Selph, K. E. and Swalethorp, R. (2021) Sinking carbon, nitrogen, and pigment flux within and beneath the euphotic zone in the oligotrophic, open-ocean Gulf of Mexico. *J. Plankton Res.*. 10.1093/plankt/fbab001.

Wada, E., Terazaki, M., Kabaya, Y. and Nemoto, T. (1987) 15 and C-13 abundances in the Antarctic Ocean with emphasis on the biogeochemical structure of the food web. *Deep Sea Res. Part A Oceanograph. Res. Paper.*, **34**, 829–841.

Wankel, S. D., Kendall, C., Pennington, J. T., Chavez, F. P. and Paytan, A. (2007) Nitrification in the euphotic zone as evidenced by nitrate dual isotopic composition: observations from Monterey Bay, California. *Global Biogeochem. Cycles*, **21**, GB2009. doi: 10.1029/2006GB002723.

Ward, B. B. and Bronk, D. A. (2001) Net nitrogen uptake and DON release in surface waters: importance of trophic interactions implied from size fractionation experiments. *Mar. Ecol. Prog. Ser.*, **219**, 11–24.

Wawrik, B., Paul, J. H., Bronk, D. A., John, D. and Gray, M. (2004) High rates of ammonium recycling drive phytoplankton productivity in the offshore Mississippi River plume. *Aquat. Microb. Ecol.*, **35**, 175–184.

Weber, S. C., Peterson, L., Battles, J. J., Roberts, B. J., Peterson, R. N., Hollander, D. J., Chanton, J. P., Joye, S. B. *et al.* (2016) Hercules 265 rapid response: immediate ecosystem impacts of a natural gas blowout incident. *Deep Sea Res. Part II*, **129**, 66–76.

Weigand, M. A., Foriel, J., Barnett, B., Oleynik, S. and Sigman, D. M. (2016) Updates to instrumentation and protocols for isotopic analysis of nitrate by the denitrifier method. *Rapid Commun. Mass Spectrom.*, **30**, 1365–1383.

Westberry, T. K., Williams, P. J. L. B. and Behrenfeld, M. J. (2012) Global net community production and the putative net heterotrophy of the oligotrophic oceans. *Global Biogeochem. Cycles*, **26**, GB4019.

White, A. E., Foster, R. A., Benitez-Nelson, C. R., Masqué, P., Verdeny, E., Popp, B. N., Arthur, K. E. and Prahl, F. G. (2013) Nitrogen fixation in the Gulf of California and the Eastern Tropical North Pacific. *Prog. Oceanogr.*, **109**, 1–17.

White, A. E., Granger, J., Selden, C., Gradoville, M. R., Potts, L., Bourbonnais, A., Fulweiler, R. W., Knapp, A. N. *et al.* (2020) A critical review of the 15N2 tracer method to measure diazotrophic production in pelagic ecosystems. *Limnol. Oceanograph.*, **18**, 129–147.

Wilson, W. D. and Johns, W. E. (1997) Velocity structure and transport in the Windward Islands passages. *Deep Sea Res. I Oceanogr. Res. Pap.*, **44**, 487–520.

Yingling, N., Kelly, T. B., Shropshire, T. A., Landry, M. R., Selph, K. E., Knapp, A. N., Kranz, S. A. and Stukel, M. R. (2021) Taxon-specific phytoplankton growth, nutrient utilization, and light limitation in the oligotrophic Gulf of Mexico. *J. Plankton Res.*.

Zhang, R., Wang, X. T., Ren, H., Huang, J., Chen, M. and Sigman, D. M. (2020) Dissolved organic nitrogen cycling in the South China Sea from an isotopic perspective. *Global Biogeochem. Cycles*, **34**, e2020GB006551.